Charge Kondo effects in a quadruple quantum dot in spinless and spinful regimes

Juho Choi, Gwangsu Yoo, Cheolhee Han, and H.-S. Sim*
Department of Physics, Korea Advanced Institute of Science and Technology, Daejeon 34141, Korea

(Received 26 October 2018; revised manuscript received 9 June 2020; accepted 9 June 2020; published 19 June 2020)

We theoretically study charge Kondo effects in a quadruple quantum dot. This system has been realized in a carbon nanotube [Nature (London) **535**, 395 (2016)] by A. Hamo *et al.*, while it can be also formed in a two-dimensional electron gas (2DEG). The system is in a particular situation where a quadruple dot has twofold degenerate ground states of ($n_A = 1, n_B = 1, n_C = 1, n_D = 0$) and (0,0,0,1) charge configurations, where n_λ is the electron occupation number of the individual dot λ = A,B,C,D of the quadruple dot. The two charge states behave as the pseudospin-1/2 states of a Kondo impurity. In the spinless regime, where the real spin of electrons is frozen, for example, by an external magnetic field, the quadruple dot can exhibit a single-channel charge Kondo effect in which coherent charge fluctuations massively occur between the two charge states with the help of electron tunneling between the quadruple dot and its electron reservoirs. The origin of the charge Kondo effect is similar to that of a negative-U Anderson impurity. In the spinful regime, on the other hand, the real spin and charge degrees of freedom couple each other due to interdot electron tunneling between the dots A and B so that the spin singlet is formed in the charge state (1,1,1,0). In this regime, the low-energy Hamiltonian of the quadruple dot system can be mapped onto a two-channel Kondo Hamiltonian having channel anisotropy. In realistic situations of carbon nanotubes or GaAs 2DEGs, the channel anisotropy is so large that the quadruple dot shows a single-channel charge Kondo effect also in the spinful regime at experimentally available temperatures. We compute the temperature dependence of electron transport through the quadruple dot, which is useful for identifying the charge Kondo effects.

DOI: 10.1103/PhysRevB.101.245307

I. INTRODUCTION

Quantum dots have been used to study various aspects of Kondo effects [1,2]. When a dot has an odd number of electrons, the nonvanishing net spin 1/2 of the electrons behaves as a Kondo impurity spin [3–5]. The Kondo effects have been observed in quantum dots in two-dimensional electron gas (2DEG) systems [6–8] and carbon nanotubes (CNTs) [9]. Experimental tunability of the dots enables one to access nontrivial features of the Kondo effects such as the scattering phase shift [10–12] and the fractional shot noise [13,14]. Furthermore, quantum dots have been used to realize exotic two-channel [15–18] and three-channel Kondo effects [19]. Quantum dots are also useful [20–23] for detecting a Kondo screening cloud [24–26]. There has been a report on experimental signatures of a Kondo cloud [27].

Kondo effects by charge or orbital degrees of freedom (rather than the spin) can appear in multiple quantum dots [28–37]. A charge Kondo effect can occur [36] in a triple dot that has two degenerate ground states of ($n_A = 1, n_B = 1, n_C = 0$) and (0,0,1) charge configurations, where n_λ is the electron occupation number in the individual dot λ = A,B,C of the triple dot. The triple dot corresponds to a negative-U Anderson impurity having negative charging energy [38]; repulsive Coulomb interactions between the dot C and the others (A and B) generate effective attractive interactions between the dots A and B, although the bare Coulomb interaction between A and B is repulsive [39]. Then at zero temperature, there occur massive charge fluctuations between (1,1,0) and (0,0,1) mediated by electron tunneling between the dot and its electron reservoirs [36]. The charge fluctuations are interpreted as the charge Kondo effect whose pseudospin impurity states are (1,1,0) and (0,0,1); in the negative-U impurity [40], the two charge states of zero and double occupancy constitute pseudospin Kondo impurity states. The (1,1,0) and (0,0,1) configurations [41] and signatures [42] of the effective attractive interactions have been experimentally observed in a triple quantum dot formed in a 2DEG, but the resulting charge Kondo effect has not been measured yet. There have been studies related to the negative-U Anderson impurity in other systems such as vibrating molecules [43–45], Josephson junctions [46,47], superconductivity in PbTe doped with Tl [48–51], and a quantum dot formed in $LaAlO_3/SrTiO_3$ interfaces [52,53].

Very recently a signature of effective attractive Coulomb interactions was observed in a quadruple quantum dot formed in two crossed CNTs [54]. This implies the possibility of a charge Kondo effect in a quadruple dot. It will be interesting to study how the charge Kondo effect occurs, its stability against deviation from the ideal setting, the resulting electron transport, and the difference from the charge Kondo effect in a triple dot.

In this work, motivated by the recent experiments [54], we investigate the charge Kondo effects in a quadruple quantum

*hssim@kaist.ac.kr

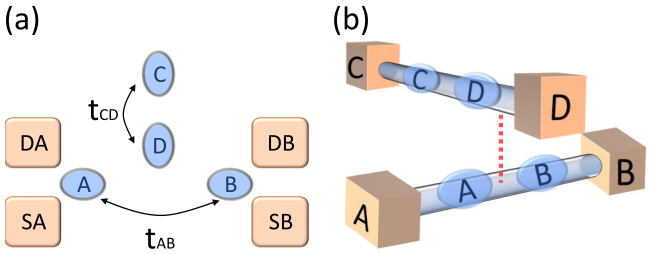

FIG. 1. (a) A quadruple dot formed in (a) a 2DEG or in (b) two crossing CNTs. Dots A, B, C, D capacitively couple to each other. The quadruple dot has a subsystem AB of the dots A and B, and the other subsystem CD of the dots C and D. In (b) a vertical dotted line is drawn to represent the relative locations of the subsystems of the CNT setup. In the subsystem AB (CD), interdot electron tunneling between A and B (C and D) occurs with strength t_{AB} (t_{CD}). There is no electron tunneling between the subsystems AB and CD. In (a), the dot A (B) couples to its source reservoir SA (SB) and drain DA (DB) via electron tunneling. In (b), each dot couples to their own reservoir depicted as a cube. The system (a) can be realized in the way reported in Refs. [34,42], while (b) was realized in Ref. [54].

dot (see Fig. 1) in the Coulomb blockade regime. We focus on the particular situation that the quadruple quantum dot has twofold degenerate ground states of ($n_A = 1, n_B = 1, n_C = 1, n_D = 0$) and (0,0,0,1) charge configurations. These degenerate charge states were experimentally realized [54]. We consider a spinless regime and a spinful regime. In the spinless regime, the real spin of electrons does not play any role in the charge Kondo effect. The spinless regime is obtained when there is no electron tunneling between the dots A and B and an external magnetic field generates sufficiently large Zeeman energy. In this regime, the electron interaction between A and B is effectively attractive, although the bare interaction is repulsive, because of the repulsive Coulomb interaction between the subsystems AB and CD. As a result, the subsystem AB behaves as a negative-U Anderson impurity, and a single-channel charge Kondo effect occurs at low temperature. We analyze the stability of the charge Kondo effect against deviation from the fixed point and compare the charge Kondo effect with that of a triple dot.

In the spinful regime, on the other hand, there is interdot electron tunneling between the dots A and B, and no external magnetic field is applied. In this regime, the real spin of electrons plays a role such that a spin singlet is formed in the subsystem AB in the charge configuration (1,1,1,0). Then the low-energy properties of the system are interestingly described by a two-channel Kondo Hamiltonian whose pseudospin-1/2 impurity states are the (1,1,1,0) charge configuration with the spin singlet and the (0,0,0,1) configuration. The Hamiltonian has anisotropy between the channels. Under realistic parameters of CNTs or GaAs 2DEGs, the channel anisotropy is so large that the quadruple dot shows a single-channel charge Kondo effect also in the spinful regime at low temperature currently achievable in experiments. For both the 2DEG and CNT systems in Fig. 1, we compute electron transport through the quadruple dot in the spinless and spinful regimes at a small source-drain bias voltage, using the Fermi liquid theory, the bosonization method, and the Fermi golden rule.

This paper is organized as follows. In Sec. II, we introduce the setup and its effective Hamiltonian. In Sec. III, we study the charge Kondo effect of a quadruple dot in the spinless regime, compare it with that of a triple dot, discuss the experimental feasibility, and compute electron transport through the quadruple dot. In Sec. IV, we show that in the spinful regime, the quadruple dot is described by a two-channel Kondo Hamiltonian with channel anisotropy. The two channels are identified and the anisotropy is estimated for quadruple dots in realistic situations. In Sec. V, we discuss summarize our findings.

II. SETUP

We introduce the quadruple dot in Fig. 1. It has a subsystem AB composed of dots A and B and the other subsystem CD of C and D. The four dots are capacitively coupled in the Coulomb blockade regime. There is no electron tunneling between the subsystems. In Fig. 1(a), electron tunneling occurs between the dot A (B) and the reservoirs SA and DA (SB and DB) of noninteracting electrons. In Fig. 1(b), A and B are formed in a CNT, and C and D are in another CNT. In this case, electron tunneling occurs between each of the four dots and its reservoir (e.g., between the dot A and the reservoir A).

The quadruple dot is described by the Hamiltonian

$$H_{\rm tot} = H_{\rm QQD} + H_{\rm res} + H_{\rm dot\text{-}res} + H_{\rm Z}. \tag{1}$$

The Hamiltonian $H_{\rm QQD}$ describes the four dot,

$$\begin{aligned} H_{\rm QQD} = & \sum_{\lambda={\rm A,B,C,D}} \sum_{\sigma=\uparrow,\downarrow} \epsilon_\lambda d^\dagger_{\lambda\sigma} d_{\lambda\sigma} \\ & + \sum_\lambda U \hat{n}_{\lambda\uparrow}\hat{n}_{\lambda\downarrow} + \frac{1}{2}\sum_{\lambda\neq\lambda'}\sum_{\sigma,\sigma'} U_{\lambda\lambda'}\hat{n}_{\lambda\sigma}\hat{n}_{\lambda'\sigma'} \\ & + \sum_\sigma t_{\rm AB} d^\dagger_{{\rm A}\sigma} d_{{\rm B}\sigma} + t_{\rm CD} d^\dagger_{{\rm C}\sigma} d_{{\rm D}\sigma} + {\rm H.c.} \end{aligned} \tag{2}$$

H.c. stands for the hermitian conjugate. Each dot $\lambda =$ A,B,C,D is modeled as an Anderson impurity having a single spinful level of energy ϵ_λ, considering strong intradot Coulomb repulsion. The operator $d^\dagger_{\lambda\sigma}$ creates an electron with spin σ in the energy level ϵ_λ. ϵ_λ can be tuned by gate voltages. $U_{\lambda\lambda'} > 0$ and $U > 0$ are inter- and intradot Coulomb repulsion energy, and $\hat{n}_{\lambda\sigma} \equiv d^\dagger_{\lambda\sigma} d_{\lambda\sigma}$ is the electron number operator of the level ϵ_λ and spin σ. For simplicity, the four dots have the same intradot Coulomb energy, the intradot Coulomb repulsion is much stronger than the interdot repulsion, $U \gg U_{\lambda\lambda'}$, and the Coulomb repulsion between dots A and C and between B and C is ignored, $U_{\rm AC} = U_{\rm BC} \sim 0$, in comparison with the other Coulomb energies. $t_{\rm AB}$ ($t_{\rm CD}$) is the strength of electron tunneling between the dots A and B (C and D). In addition, we consider the A-B symmetric case,

$$\epsilon_{\rm A} = \epsilon_{\rm B} \equiv \epsilon_0, \qquad U_{\rm AD} = U_{\rm BD} \equiv V. \tag{3}$$

Relaxing the above simplifications does not alter our results qualitatively, provided that the twofold ground-state degeneracy is maintained. The condition for the twofold degeneracy will be discussed in Sec. III A.

The second term $H_{\rm res}$ of Eq. (1) is for the reservoirs of noninteracting electrons. The reservoirs of the 2DEG setup

in Fig. 1(a) are described by

$$H_{\rm res}^{\rm 2DEG} = \sum_{\eta={\rm S,D}} \sum_{\lambda={\rm A,B}} \sum_{\vec{k},\sigma} \epsilon_{\eta\lambda\vec{k}} c^{\dagger}_{\eta\lambda\vec{k}\sigma} c_{\eta\lambda\vec{k}\sigma}. \tag{4}$$

The operator $c^{\dagger}_{\eta\lambda\vec{k}\sigma}$ creates an electron with wave vector $\vec{k}$, spin σ, and energy $\epsilon_{\eta\lambda\vec{k}}$ in reservoir $\eta\lambda$. On the other hand, the CNT setup in Fig. 1(b) has a different configuration of reservoirs from the 2DEG setup. The reservoirs of the CNT setup are described by

$$H_{\rm res}^{\rm CNT} = \sum_{\lambda={\rm A,B,C,D}} \sum_{\vec{k},\sigma} \epsilon_{\lambda\vec{k}} \tilde{c}^{\dagger}_{\lambda\vec{k}\sigma} \tilde{c}_{\lambda\vec{k}\sigma}. \tag{5}$$

The operator $\tilde{c}^{\dagger}_{\lambda\vec{k}\sigma}$ creates an electron with wave vector $\vec{k}$, spin σ, and energy $\epsilon_{\lambda\vec{k}}$ in CNT reservoir λ.

The third term $H_{\rm dot\text{-}res}$ of Eq. (1) describes electron tunneling between the dots and the reservoirs. For the 2DEG setup in Fig. 1(a), it is written as

$$\begin{aligned} H_{\rm dot\text{-}res}^{\rm 2DEG} &= t_0 \sum_{\eta={\rm S,D}} \sum_{\lambda={\rm A,B}} \sum_{\vec{k},\sigma} d^{\dagger}_{\lambda\sigma} c_{\eta\lambda\vec{k}\sigma} + {\rm H.c.} \\ &= \sqrt{2} t_0 \sum_{\lambda={\rm A,B}} \sum_{\vec{k},\sigma} d^{\dagger}_{\lambda\sigma} c_{\lambda\vec{k}\sigma} + {\rm H.c.}, \end{aligned} \tag{6}$$

where t_0 is the tunneling strength. For simplicity, the electron tunneling strength from dot λ to its source reservoir Sλ is the same as that to the drain Dλ, and its dependence on $\vec{k}$ is ignored. In the second line of the above equation, we introduce the symmetric combination

$$c^{\dagger}_{\lambda\vec{k}\sigma} \equiv \frac{1}{\sqrt{2}} (c^{\dagger}_{{\rm S}\lambda\vec{k}\sigma} + c^{\dagger}_{{\rm D}\lambda\vec{k}\sigma}) \tag{7}$$

of operators of the source and drain of dot λ. It describes the reservoir electrons hybridized to the dot by the tunneling. For the CNT setup in Fig. 1(b), on the other hand, electron tunneling between the dots and the reservoirs is described by

$$\begin{aligned} H_{\rm dot\text{-}res}^{\rm CNT} &= \sqrt{2} t_0 \sum_{\lambda={\rm A,B}} \sum_{\vec{k},\sigma} d^{\dagger}_{\lambda\sigma} \tilde{c}_{\lambda\vec{k}\sigma} + {\rm H.c.} \\ &\quad + t_1 \sum_{\lambda={\rm C,D}} \sum_{\vec{k},\sigma} d^{\dagger}_{\lambda\sigma} \tilde{c}_{\lambda\vec{k}\sigma} + {\rm H.c.} \end{aligned} \tag{8}$$

Here, $\sqrt{2}$ is put to make the form of Eq. (8) the same as that of Eq. (6). t_0 is the strength of tunneling between dot A and reservoir A and between dot B and reservoir B, while t_1 is the tunneling strength between dot C and reservoir C and between dot D and reservoir D. The last term $H_{\rm Z}$ of Eq. (1) describes the Zeeman spin splitting $E_{\rm Z}$ of the energy level of each dot, which appears in the presence of an external magnetic field,

$$H_{\rm Z} = \sum_{\lambda={\rm A,B,C,D}} E_{\rm Z} \frac{\hat{n}_{\lambda\uparrow} - \hat{n}_{\lambda\downarrow}}{2}. \tag{9}$$

III. SINGLE-CHANNEL CHARGE KONDO EFFECTS IN THE SPINLESS REGIME

In this section, we consider the spinless regime of $t_{\rm AB} = 0$ and sufficiently large Zeeman energy $E_{\rm Z}$. In this regime, we can ignore the effects of spins, such as the ordinary spin Kondo effects of each of the dots A and B. We show below that the twofold degenerate ground states of (1,1,1,0) and (0,0,0,1) charge configurations of the quadruple dot behave as pseudospin states and that the Hamiltonian in Eq. (1) is transformed into an anisotropic Kondo Hamiltonian of the pseudospin. We compute electron transport through the quadruple dot for both the 2DEG and CNT cases.

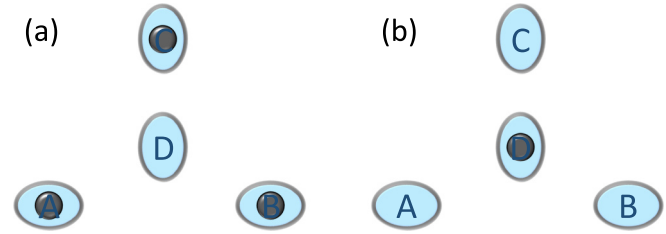

FIG. 2. Pseudospins of the quadruple dot in the spinless regime of $E_{\rm Z} \neq 0$ and $t_{\rm AB} = 0$. (a) The charge configuration (1,1,1,0) corresponds to the pseudospin up. (b) The charge configuration (0,0,0,1) corresponds to the pseudospin down.

A. Parameter regime and pseudospin

We consider large Zeeman energy $E_{\rm Z}$ due to an external magnetic field. When $E_{\rm Z}$ is larger than $|\epsilon_0 + U_{\rm AB}|$, $|\epsilon_0 + V|$, and V, the Zeeman energy is bigger than energy difference between the ground states and the excited states such as $(n_{\rm A} = 1, n_{\rm B} = 0, n_{\rm C} = 1, n_{\rm D} = 0)$ and (0,0,1,0) charge configurations. $E_{\rm Z}$ is also larger than the Kondo temperature $T_{K,{\rm spin}}$ of the ordinary spin Kondo effect of the dot A or B. Then spin effects are suppressed, and we can treat the quadruple dot as a spinless system in its low-energy regime. In the spinless regime, we replace the spinful operators of the Hamiltonian in Eq. (1) by corresponding spinless ones, $d_{\lambda\sigma} \to d_\lambda$, $c_{\lambda\vec{k}\sigma} \to c_{\lambda\vec{k}}$, and $\tilde{c}_{\lambda\vec{k}\sigma} \to \tilde{c}_{\lambda\vec{k}}$.

We discuss the conditions for the quadruple dot to have the degenerate ground states of (1,1,1,0) and (0,0,0,1) charge configurations. We need $2\epsilon_0 + \epsilon_{\rm C} + U_{\rm AB} = \epsilon_{\rm D}$, with which the two configurations have the same energy. We also need $0 < \epsilon_{\rm C} - \epsilon_{\rm D} < 2V$ and $-V < \epsilon_0 < -U_{\rm AB}$, with which the two configurations have lower energy than the other configurations such as (1,0,0,1) and (1,0,1,0). In addition, the energy difference between the ground states and excited states has to be larger than the level broadening $\Gamma = \pi \rho t_0^2$ of the states. Γ is induced by electron tunneling between the dots and the reservoirs, and ρ is the density of reservoir states at the Fermi level. The degeneracy conditions can be achieved in experiments by exploring the charge stability diagram with tuning gate voltages. Indeed, the degenerate ground states have been achieved in a recent experiment [54] of a quadruple dot in CNTs. For computational convenience, we choose an additional condition of $\epsilon_{\rm D} + V = \epsilon_{\rm C}$. Relaxation of this condition does not alter our results qualitatively.

The twofold degenerate ground-state charge configurations (1,1,1,0) and (0,0,0,1) behave as pseudospin-up and -down states, respectively (see Fig. 2),

$$|\Uparrow\rangle = d^{\dagger}_{\rm A} d^{\dagger}_{\rm B} d^{\dagger}_{\rm C} |0\rangle, \quad |\Downarrow\rangle = d^{\dagger}_{\rm D} |0\rangle. \tag{10}$$

$|0\rangle$ is the vacuum state of the quadruple dot. Accordingly, we define pseudospin-1/2 operators, $\tau_+ = |\Uparrow\rangle\langle\Downarrow|$, $\tau_- = |\Downarrow\rangle\langle\Uparrow|$, and $\tau_z = (|\Uparrow\rangle\langle\Uparrow| - |\Downarrow\rangle\langle\Downarrow|)/2$ for later use.

B. Single-channel Kondo Hamiltonian

For the 2DEG setup [Fig. 1(a)], we transform, under the conditions discussed above, the Hamiltonian in Eq. (1) into a low-energy effective Hamiltonian $H_{\rm eff1}$, by applying the Schrieffer-Wolff transformation [55] and using the pseudospin operators τ's in Eq. (10),

$$\begin{aligned} H_{\rm eff1}^{\rm 2DEG} &= \sum_{\vec{k},\vec{k}'} J_z \tau_z (c^\dagger_{{\rm A}\vec{k}} c_{{\rm A}\vec{k}'} + c^\dagger_{{\rm B}\vec{k}} c_{{\rm B}\vec{k}'}) \\ &\quad + \left(\sum_{\vec{k},\vec{k}'} J_+ \tau_+ c_{{\rm B}\vec{k}} c_{{\rm A}\vec{k}'} + {\rm H.c.} \right) + H_{\rm res}^{\rm 2DEG}, \\ J_z &= \frac{4t_0^2}{\epsilon_0 + V}, \quad J_+ = -\frac{4t_0^2 t_{\rm CD}}{\epsilon_0 + V} \left(\frac{2}{V} + \frac{1}{\epsilon_0 + V} \right). \end{aligned} \tag{11}$$

Then, we (i) apply the particle-hole transformation to electrons in reservoirs ηB,

$$c_{\eta{\rm B}\vec{k}} \to c^\dagger_{\eta{\rm B}\vec{k}}, \quad \epsilon_{\eta{\rm B}\vec{k}} \to -\epsilon_{\eta{\rm B}\vec{k}}, \tag{12}$$

and (ii) assign pseudospin-up $\Uparrow$ to electrons in reservoirs ηA and pseudospin-down $\Downarrow$ to those in reservoirs ηB, namely $\eta{\rm A} \to \Uparrow$, $\eta{\rm B} \to \Downarrow$. Then $H_{\rm eff1}$ becomes the standard form of the single-channel Kondo effect,

$$\begin{aligned} H_{\rm 1ch}^{\rm 2DEG} &= H_{\rm res}^{\rm 2DEG} + 2J_z \tau_z s_z + J_+ \tau_+ s_- + {\rm H.c.}, \\ s_{i=x,y,z} &= \sum_{\mu,\mu'=\Uparrow,\Downarrow} \sum_{\vec{k},\vec{k}'} c^\dagger_{\mu\vec{k}} \frac{\sigma^i_{\mu\mu'}}{2} c_{\mu'\vec{k}'}, \quad s_\pm = s_x \pm i s_y, \end{aligned} \tag{13}$$

where $\sigma^{i=x,y,z}$'s are the Pauli matrices for the pseudospins of the reservoir electrons. This indicates that a Kondo effect of the pseudospin can occur.

In the same way, we also obtain a low-energy effective Hamiltonian $H_{\rm 1ch}$ for the CNT setup [Fig. 1(b)]. In the absence of electron tunneling between the quadruple dot and the reservoirs C and D [i.e., the case of $t_1 = 0$ in Eq. (8)], the low-energy effective Hamiltonian has the same form as that of the 2DEG setup but with replacement of $c_{\mu\vec{k}} \to \tilde{c}_{\mu\vec{k}}$ and $H_{\rm res}^{\rm 2DEG} \to H_{\rm res}^{\rm CNT}$, hence it shows the same pseudospin Kondo effect. The case of $t_1 \neq 0$ will be discussed in Sec. III D.

The pseudospin Kondo effect means that coherent fluctuations massively occur between the two charge configurations (1,1,1,0) and (0,0,0,1) with the help of electron tunneling between the dot and the reservoirs. It is reminiscent of the charge Kondo effect [40] of a negative-U Anderson impurity. The subsystem AB of the quadruple dot behaves as a negative-U impurity, as it prefers double electron occupancy $n_{\rm A} + n_{\rm B} = 2$ [for the ground-state charge configuration ($n_{\rm A} = 1, n_{\rm B} = 1, n_{\rm C} = 1, n_{\rm D} = 0$)] and zero occupancy $n_{\rm A} + n_{\rm B} = 0$ [for (0,0,0,1)]. This implies that electron interaction between the dots A and B is effectively attractive, although the bare interaction is repulsive; the effective attractive interaction between the dots A and B occurs due to the repulsive Coulomb interaction between the subsystems AB and CD.

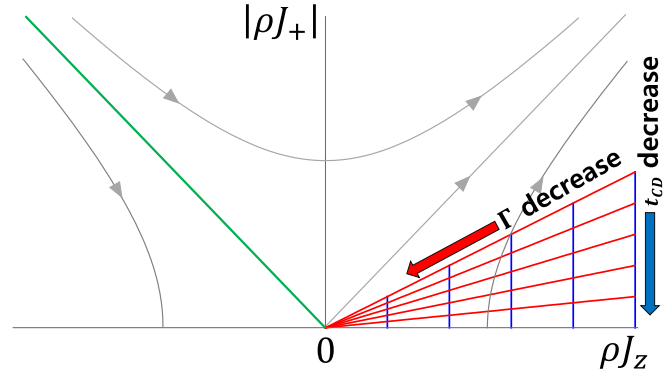

FIG. 3. Phase diagram of the anisotropic Kondo Hamiltonian in Eq. (13). The renormalization group flows of the coupling strengths J_z and J_+ are drawn by thin arrows. The phase transition line between the antiferromagnetic Kondo phase and the ferromagnetic phase is shown by the green solid line. The shaded region is the anisotropy domain achievable by tuning the tunneling strengths $t_{\rm CD}$ (along the thick blue arrow) and t_0 (equivalently, $\Gamma = \pi\rho t_0^2$, along the thick red arrow).

The Kondo Hamiltonian in Eq. (13) has pseudospin anisotropy $J_z \neq J_+$ due to the fact that pseudospin flip and nonflip processes have different amplitude, $J_z > J_+$. The pseudospin flip $(1,1,1,0) \leftrightarrow (0,0,0,1)$, contributing to J_+, is accompanied by three electron-tunneling events, one between the dots C and D, another between the dot A and its reservoirs A, and the other between the dot B and its reservoirs B. By contrast, pseudospin nonflip, contributing to J_z, involves two tunneling events, one from dot λ (=A,B) to reservoirs λ and the other from reservoirs λ to dot λ.

It should be mentioned that J_z is always positive, as shown in Eq. (11). Hence the quadruple dot approaches the strong coupling Kondo fixed point of antiferromagnetic screening for any values of t_0, ϵ_0, V, and $t_{\rm CD}$ in the spinless regime (see Fig. 3). It cannot show the ferromagnetic phase of the usual anisotropic Kondo Hamiltonian [2,56]. So the charge Kondo effect is stable at low temperature.

We compare these findings with the charge Kondo effect [36] of a triple quantum dot. The charge Kondo effect in a triple dot is also pseudospin anisotropic, as its pseudospin-flip processes are of higher order in electron tunneling than pseudospin nonflip, similarly to the quadruple dot. However, the coupling strength J_z can be negative in the triple dot, so that the ferromagnetic phase and the phase transition between the ferromagnetic phase and the antiferromagnetic Kondo phase can be explored in the triple dot. This happens because the anisotropic charge Kondo effect of the triple dot is accompanied by three different electron species (corresponding to the dots A, B, C of the triple dot). By contrast, in the quadruple dot, only two species of electrons (corresponding to the dots A and B) are involved, and only the antiferromagnetic Kondo phase can emerge.

C. Electron transport in the 2DEG setup

In this subsection, we consider the quadruple dot of the 2DEG setup in Fig. 1(a) and study electron transport through

the quadruple dot in the single-channel charge Kondo regime of the spinless case. By using the scattering T-matrix method, the Fermi liquid theory and the Poorman's scaling, we compute electron current through the dot A from its source SA to its drain DA both in the strong Kondo coupling regime at low temperature and the weak Kondo coupling regime at high temperature. We also estimate the Kondo temperature T_K of the charge Kondo effect at the end of the subsection.

The current $I_{\rm A}$ through the dot A is computed when bias voltages $V_{\rm A}/2$ and $V_{\rm B}/2$ are applied to the sources SA and SB, respectively, while $-V_{\rm A}/2$ and $-V_{\rm B}/2$ to the drains DA and DB, respectively. It is expressed [57] as

$$\begin{aligned} I_{\rm A} &= \frac{ie}{\hbar}\int \frac{d\epsilon}{2\pi}\pi\rho t_0^2\big[G^r_{\rm A}(\epsilon)-G^a_{\rm A}(\epsilon)\big](f_{\rm SA}(\epsilon)-f_{\rm DA}(\epsilon)) \\ &= \frac{-e}{h}\int d\epsilon\big[\pi\rho{\rm Im}\big(T^c_{\rm A}(\epsilon)\big)\big](f_{\rm SA}(\epsilon)-f_{\rm DA}(\epsilon)). \end{aligned} \tag{14}$$

$f_{\eta{\rm A}}$ is the Fermi-Dirac distribution of reservoir ηA. $G^{r(a)}_{\rm A}(\epsilon)$ is the retarded (advanced) Green function of the dot A in the energy ϵ domain. $T^c_{\rm A}(\epsilon)$ is the T matrix of reservoir electrons $c^\dagger_{{\rm A}\vec{k}}$, satisfying $G^r_{{\rm A}\vec{k}}(\epsilon)=G^{0r}_{{\rm A}\vec{k}}(\epsilon)+G^{0r}_{{\rm A}\vec{k}}(\epsilon)T^c_{\rm A}(\epsilon)G^{0r}_{{\rm A}\vec{k}}(\epsilon)$. $G^r_{{\rm A}\vec{k}}$ ($G^{0r}_{{\rm A}\vec{k}}$) is the Green function of the reservoir electrons in the presence (absence) of electron tunneling between the dot A and reservoirs ηA. In the last step of Eq. (14) we use $T^c_{\rm A}(\epsilon)=(\sqrt{2}t_0)^2G^r_{\rm A}(\epsilon)$ derived by using the equation of motion.

In the strong Kondo coupling regime at low temperature $T\ll T_K$ and at small bias voltages $eV_{\rm A}$, $eV_{\rm B}\ll k_BT_K$, the current in Eq. (14) is computed using the Fermi liquid theory, where k_B is the Boltzmann constant. According to Nozieres [58], the Fermi liquid near the Kondo fixed point is described by quasiparticles $b^\dagger_{\mu\vec{k}}$ of pseudospin μ, momentum $\vec{k}$, and energy $\epsilon_{\vec{k}}$. The fixed-point Hamiltonian is

$$\begin{aligned} H_{\rm fp} &= H_{\rm res}-\frac{\alpha}{\pi\rho T_K}\sum_{\vec{k},\vec{k}',\mu=\Uparrow,\Downarrow}\left(\frac{\epsilon_{\mu\vec{k}}+\epsilon_{\mu\vec{k}'}}{2}\right)b^\dagger_{\mu\vec{k}}b_{\mu\vec{k}'} \\ &\quad+\frac{\beta}{\pi\rho^2T_K}\sum_{\vec{k}_1,\vec{k}_2,\vec{k}_3,\vec{k}_4} b^\dagger_{\Uparrow\vec{k}_1}b_{\Uparrow\vec{k}_2}b^\dagger_{\Downarrow\vec{k}_3}b_{\Downarrow\vec{k}_4}. \end{aligned} \tag{15}$$

The α terms describe elastic scattering of the quasiparticles and the β terms are for inelastic scattering due to interactions between the quasiparticles. The coefficients satisfy $\alpha=\beta=1$, according to the Nozieres theory. We restore the index $\lambda=$ A,B and perform the inverse of the transformation in Eq. (12), $b_{\Uparrow\vec{k}}\to b_{{\rm A}\vec{k}}$, $b_{\Downarrow\vec{k}}\to b^\dagger_{{\rm B}\vec{k}}$, and $\epsilon_{\Downarrow\vec{k}}\to-\epsilon_{{\rm B}\vec{k}}$. The transformation results in

$$\begin{aligned} H_{\rm fp} &\to H_{\rm res}-\frac{\alpha}{\pi\rho T_K}\sum_{\vec{k},\vec{k}';\lambda={\rm A,B}}\left(\frac{\epsilon_{\lambda\vec{k}}+\epsilon_{\lambda\vec{k}'}}{2}\right)b^\dagger_{\lambda\vec{k}}b_{\lambda\vec{k}'} \\ &\quad-\frac{\beta}{\pi\rho^2T_K}\sum_{\vec{k}_1,\vec{k}_2,\vec{k}_3,\vec{k}_4} b^\dagger_{{\rm A}\vec{k}_1}b_{{\rm A}\vec{k}_2}b^\dagger_{{\rm B}\vec{k}_3}b_{{\rm B}\vec{k}_4}, \\ b_{{\rm A}\vec{k}} &= \frac{1}{\sqrt{2}}(b_{{\rm SA}\vec{k}}+b_{{\rm DA}\vec{k}}),\quad b_{{\rm B}\vec{k}}=\frac{1}{\sqrt{2}}(b_{{\rm SB}\vec{k}}+b_{{\rm DB}\vec{k}}). \end{aligned} \tag{16}$$

The last equations for $b_{\lambda\vec{k}}$ and $\epsilon_{\lambda\vec{k}}=\epsilon_{{\rm S}\lambda\vec{k}}=\epsilon_{{\rm D}\lambda\vec{k}}$ are naturally chosen, based on the one-to-one correspondence between $b_{\lambda\vec{k}}$ and $c_{\lambda\vec{k}}$ [see Eq. (7) for $c_{\lambda\vec{k}}$]. The minus sign in front of the β terms implies [36] effective attractive interactions of electrons between reservoirs ηA and ηB.

The T-matrix $T^c_{\rm A}$ of the $c_{{\rm A}\vec{k}}$ reservoir electrons in Eq. (14) is related to the corresponding T-matrix $T^b_{\rm A}$ of the $b_{{\rm A}\vec{k}}$ quasiparticles at their Fermi level [59], defined by $\mathcal{G}^r_{{\rm A}\vec{k}}(\epsilon)=\mathcal{G}^{0,r}_{{\rm A}\vec{k}}(\epsilon)+\mathcal{G}^{0,r}_{{\rm A}\vec{k}}(\epsilon)T^b_{\rm A}(\epsilon)\mathcal{G}^{0,r}_{{\rm A}\vec{k}}(\epsilon)$, where $\mathcal{G}^r_{{\rm A}\vec{k}}$ ($\mathcal{G}^{0,r}_{{\rm A}\vec{k}}$) is the retarded Green function of the $b_{{\rm A}\vec{k}}$ quasiparticles in the presence (absence) of the scattering by the α and β terms of $H_{\rm fp}$. The T matrices have the form of $\exp(2i\delta_{b,c}(\epsilon))=1-2\pi i\rho T^{b,c}_{\rm A}(\epsilon)$, according to the scattering theory, and the scattering phase shift $\delta_c(\epsilon)$ of the $c_{{\rm A}\vec{k}}$ reservoir electrons is different from the scattering phase shift $\delta_b(\epsilon)$ of the $b_{{\rm A}\vec{k}}$ quasiparticles by constant $\pi/2$, $\delta_c(\epsilon)=\delta_b(\epsilon)+\pi/2$. These lead to

$$-{\rm Im}\big[\pi\rho T^c_{\rm A}(\epsilon)\big]=1+{\rm Im}\big[\pi\rho T^b_{\rm A}(\epsilon)\big]. \tag{17}$$

Using the fixed-point Hamiltonian $H_{\rm fp}$ and applying the equation of motion method to $\mathcal{G}^r_{{\rm A}\vec{k}}$, we compute the T-matrix $T^b_{\rm A}$ of the $b_{{\rm A}\vec{k}}$ quasiparticles up to the second order terms of α and β, in terms of $F_\lambda(\epsilon)\equiv(f_{{\rm S}\lambda}(\epsilon)+f_{{\rm D}\lambda}(\epsilon))/2$,

$$\begin{aligned} {\rm Im}\big[T^b_{\rm A}(\epsilon)\big] &= -\frac{\alpha^2}{\pi\rho T_K^2}\epsilon^2 \\ &\quad-\frac{\beta^2}{\pi\rho T_K^2}\int d\epsilon_{\vec{k}_1}d\epsilon_{\vec{k}_2}\big[\big(1-F_{\rm A}(\epsilon_{\vec{k}_1})\big)F_{\rm B}(\epsilon_{\vec{k}_2}) \\ &\quad\times\big(1-F_{\rm B}(\epsilon-\epsilon_{\vec{k}_1}+\epsilon_{\vec{k}_2})\big)+F_{\rm A}(\epsilon_{\vec{k}_1}) \\ &\quad\times\big(1-F_{\rm B}(\epsilon_{\vec{k}_2})\big)F_{\rm B}(\epsilon-\epsilon_{\vec{k}_1}+\epsilon_{\vec{k}_2})\big]. \end{aligned} \tag{18}$$

Combining Eqs. (14), (17), (18), and $\alpha=\beta=1$, we obtain the electron current $I_{\rm A}$ through the dot A at zero temperature as a function of the voltages $V_{\rm A}$ and $V_{\rm B}$,

$$I_{\rm A}=\frac{e^2}{h}V_{\rm A}\left[1-\frac{1}{4}\left(\frac{eV_{\rm A}}{k_BT_K}\right)^2-\frac{1}{4}\left(\frac{eV_{\rm B}}{k_BT_K}\right)^2+O\left(\left(\frac{V_{\rm A,B}}{T_K}\right)^3\right)\right]. \tag{19}$$

The zero-bias differential conductance through the dot A at temperature T (when $V_{\rm A}=V_{\rm B}\to0$) is found,

$$\frac{dI_{\rm A}}{dV_{\rm A}}=\frac{e^2}{h}\left[1-\left(\frac{T}{T_K}\right)^2\right]. \tag{20}$$

The power-law exponent 2 is a feature of the Fermi liquid.

In the weak coupling regime at high temperature $T\gg T_K$, on the other hand, the current in Eq. (14) can be computed by treating J_z and J_+ in Eq. (11) perturbatively. From the relation $G^r_{{\rm A}\vec{k}}(\epsilon)=G^{0r}_{{\rm A}\vec{k}}(\epsilon)+G^{0r}_{{\rm A}\vec{k}}(\epsilon)T^c_{\rm A}(\epsilon)G^{0r}_{{\rm A}\vec{k}}(\epsilon)$ at electron energy ϵ, we compute the T-matrix $T^c_{\rm A}(\epsilon)$ of reservoir electrons $c^\dagger_{{\rm A}\vec{k}}$ in Eq. (14).

$${\rm Im}\big[T^c_{\rm A}(\epsilon)\big]=-\frac{\pi\rho}{4}\big[J_z^2(\epsilon)+2J_+^2(\epsilon)\big]. \tag{21}$$

We express $J_z(\epsilon)$ in terms of the Kondo temperature T_K, using the Poorman's scaling at $\epsilon\gtrsim T_K$,

$$J_z(\epsilon)=J_\Delta\frac{(1+(\epsilon/T_K)^{-4\rho J_\Delta})}{(1-(\epsilon/T_K)^{-4\rho J_\Delta})}, \tag{22}$$

where $J_\Delta\equiv\sqrt{J_z^2-J_+^2}$ is the bare anisotropy strength [see Eq. (11)], and $J_+(\epsilon)$ satisfies $J_+^2(\epsilon)=J_z^2(\epsilon)-J_\Delta^2$. Using

Eqs. (14), (21), and (22), we obtain the electron conductance through the dot A in the zero-bias limit of $V_A = V_B \to 0$ at high temperature $T \gg T_K$,

$$\frac{dI_A}{dV_A} = \frac{e^2\pi^2\rho^2}{4h} J_\Delta^2 \left[3\left(\frac{(1+(T/T_K)^{-4\rho J_\Delta})}{(1-(T/T_K)^{-4\rho J_\Delta})} \right)^2 - 2 \right]. \quad (23)$$

This result has the same form as that of an anisotropic Kondo model in Ref. [36]. When the anisotropy strength becomes zero ($J_\Delta \to 0$), the conductance shows logarithmic behavior as in the case of usual Kondo effects; $dI_A/dV_A \propto 1/(\ln(T/T_K))^2$.

We estimate the Kondo temperature T_K of the charge Kondo effect in a quadruple dot of the 2DEG setup [Fig. 1(a)]. It follows the standard expression of the anisotropic Kondo effects [36],

$$T_K = D_0 \left(\frac{J_z + J_\Delta}{J_z - J_\Delta} \right)^{-1/4\rho J_\Delta}. \quad (24)$$

Here, D_0 is the bare bandwidth of the reservoirs. We find that T_K can reach about 100 mK. This is estimated with the realistic parameters [34,42] of $V \sim 0.2$–0.4 meV, $U_{AB} \sim 0.05$–0.2 meV, $t_{CD} \sim 5$–70 μeV, and $\Gamma \sim 1$–50 μeV.

D. Electron transport in the CNT setup

In this subsection, we consider the quadruple dot of the CNT setup [see Fig. 1(b)] in the single-channel charge Kondo regime of the spinless case. We compute electron current I_{CD} from the reservoir D to C through the dots C and D in the limit of zero bias, by using the bosonization and refermionization method as well as the Fermi golden rule when the tunneling strength t_1 between the dot C and the reservoir C and between the dot D and the reservoir D is sufficiently weak. We also estimate the Kondo temperature T_K of the charge Kondo effect of the CNT setup at the end of the subsection. We note that the current I_{CD} can be measured as in Ref. [54].

For the CNT setup, the low-energy effective Hamiltonian has more terms than the Hamiltonian of the 2DEG setup in Eq. (13), when the tunneling strength t_1 is nonzero. Using the Schreiffer-Wolff transformation, we find that the effective Hamiltonian is decomposed into

$$\begin{aligned}
H_{CNT} &= H_{eff1}^{CNT} + H_{Pz} + H_{P+}, \\
H_{eff1}^{CNT} &= H_{res}^{CNT} + 2J_z\tau_z s_z + J_+\tau_+ s_- + \text{H.c.}, \\
H_{Pz} &= \sum_{\vec{k},\vec{k}'} J_{Pz}\tau_z(\tilde{c}^\dagger_{C\vec{k}}\tilde{c}_{C\vec{k}'} - \tilde{c}^\dagger_{D\vec{k}}\tilde{c}_{D\vec{k}'}) \\
H_{P+} &= \sum_{\vec{k}_1,\vec{k}_2,\vec{k}_3,\vec{k}_4} J_{P+}\tau_+ \tilde{c}_{B\vec{k}_1}\tilde{c}_{A\vec{k}_2}\tilde{c}^\dagger_{D\vec{k}_3}\tilde{c}_{C\vec{k}_4} + \text{H.c.}, \\
s_i &= \sum_{\mu,\mu'=\Uparrow,\Downarrow} \sum_{\vec{k},\vec{k}'} \tilde{c}^\dagger_{\mu\vec{k}} \frac{\sigma^i_{\mu\mu'}}{2} \tilde{c}_{\mu'\vec{k}'}, \quad s_\pm = s_x \pm i s_y, \\
J_{Pz} &= \frac{t_1^2}{2}\left(\frac{1}{V-\epsilon_C} + \frac{1}{\epsilon_C + V + U_{CD}} \right), \\
J_{P+} &= \frac{4t_0^2 t_1^2 U_{CD}(2\epsilon_0 + 3V)}{\epsilon_C(\epsilon_C + U_{CD})V(\epsilon_0 + V)^2}.
\end{aligned} \quad (25)$$

The first term H_{eff1}^{CNT} of the effective Hamiltonian H_{CNT} has the same form with the effective Hamiltonian H_{eff1}^{2DEG} of the 2DEG setup in Eq. (11), and it describes the single-channel charge Kondo effect. The other two terms H_{Pz} and H_{P+} occur when electron tunneling happens between the dot C and the reservoir C and between the dot D and the reservoir D, namely when $t_1 \neq 0$. H_{P+} describes processes of pseudospin flip, while H_{Pz} describes processes of pseudospin nonflip. Here, a process of pseudospin flip, for example, from $|\Downarrow\rangle$ to $|\Uparrow\rangle$ happens such that electron tunneling occurs from the reservoir C to the dot C, another tunneling from the dot D to the reservoir D, another tunneling from the reservoir A to the dot A, and the other from the reservoir B to the dot B.

We compute the current I_{CD} when very low bias voltages $V_{CD}/2$ and $-V_{CD}/2$ are applied to the reservoirs D and C, respectively; we consider the limit of $V_{CD} \to 0$. We focus on the regime of sufficiently weak t_1 where the single-channel charge Kondo effect is perturbatively affected by the two terms $H_{Pz} + H_{P+}$ induced by the tunneling t_1. The current I_{CD} is expressed as

$$I_{CD} = -e(\Gamma^{C\leftarrow D} - \Gamma^{D\leftarrow C}). \quad (26)$$

$\Gamma^{C\leftarrow D}$ is the rate of electron transfer from the reservoir D to the reservoir C, while $\Gamma^{D\leftarrow C}$ is the rate of electron transfer from the reservoir C to the reservoir D.

To calculate $\Gamma^{C\leftarrow D}$ and $\Gamma^{D\leftarrow C}$, we bosonize and then refermionize [60] the Hamiltonian H_{CNT} in Eq. (25). The details of the bosonization and refermionization are given in Appendix. The resulting Hamiltonian at the Toulouse point [60] is found as

$$\begin{aligned}
H_{EK} &= H_{0K} + H_{0C} + H_{0D} + H'_{Pz} + H'_{P+} + \text{constant}, \\
H_{0K} &= \sum_{\vec{k}} \epsilon_{\vec{k}} \tilde{c}^\dagger_{\vec{k}} \tilde{c}_{\vec{k}} + V_K \sum_{\vec{k}} (\tilde{c}^\dagger_d \tilde{c}_{\vec{k}} + \tilde{c}^\dagger_{\vec{k}} \tilde{c}_d) \\
&= \sum_{\epsilon} \epsilon \tilde{c}^\dagger_\epsilon \tilde{c}_\epsilon, \\
H_{0C} &= \sum_{\vec{k}} \epsilon_{C\vec{k}} \tilde{c}^\dagger_{C\vec{k}} \tilde{c}_{C\vec{k}}, \\
H_{0D} &= \sum_{\vec{k}} \epsilon_{D\vec{k}} \tilde{c}^\dagger_{D\vec{k}} \tilde{c}_{D\vec{k}}, \\
H'_{Pz} &= \sum_{\vec{k},\vec{k}'} J_{Pz}(\tilde{c}^\dagger_d \tilde{c}_d - 1/2)(\tilde{c}^\dagger_{C\vec{k}} \tilde{c}_{C\vec{k}'} - \tilde{c}^\dagger_{D\vec{k}} \tilde{c}_{D\vec{k}'}), \\
H'_{P+} &= V_P \sum_{\vec{k}_1,\vec{k}_2,\vec{k}_3} \tilde{c}^\dagger_d \tilde{c}_{\vec{k}_1} \tilde{c}^\dagger_{D\vec{k}_2} \tilde{c}_{C\vec{k}_3} + \text{H.c.}
\end{aligned} \quad (27)$$

H_{0K} is obtained from the charge Kondo Hamiltonian H_{eff1}^{CNT} of Eq. (11). $\tilde{c}_d$ flips the pseudospin of the quadruple dot from up to down, and $\tilde{c}^\dagger_{\vec{k}}$ creates an electron with momentum $\vec{k}$ in an electron bath that combines the reservoirs A and B. H_{0K} is diagonalized in energy basis as $\sum_\epsilon \epsilon \tilde{c}^\dagger_\epsilon \tilde{c}_\epsilon$. H_{0C} and H_{0D} are the Hamiltonian of the reservoirs C and D. H'_{Pz} and H'_{P+} are obtained from the Hamiltonian H_{Pz} and H_{P+} of Eq. (25), respectively, and describe processes accompanied by electron tunneling t_1 between the quadruple dot and the reservoirs C and D. The coupling amplitudes V_K and V_P satisfy $V_K \propto J_+$ and $V_P \propto J_{P+}$.

We calculate $\Gamma^{C\leftarrow D}$ and $\Gamma^{D\leftarrow C}$, using the Fermi golden rule and treating H'_{P_z} and H'_{P+} as a perturbation of the exactly solvable Hamiltonian $H_{0K}+H_{0C}+H_{0D}$. The perturbation is a valid approach for sufficiently small $J_{Pz}, J_{P+} \propto t_1^2$, since H'_{P_z} and H'_{P+} are irrelevant according to a scaling analysis (see Appendix). The lowest-order Fermi golden rule expression of $\Gamma^{C\leftarrow D}$ is

$$\Gamma^{C\leftarrow D} = 2\pi \sum_{|f\rangle,|i\rangle} |\langle f|H'_{P+}|i\rangle|^2 W_i \delta(E_i - E_f). \tag{28}$$

Here, the summation runs over all possible initial states $|i\rangle$ with energy E_i and final states $|f\rangle$ with energy E_f. $|i\rangle$ and $|f\rangle$ are eigenstates of $H_{0K}+H_{0C}+H_{0D}$ and contribute to $\Gamma^{C\leftarrow D}$ when they are related as

$$|f\rangle = \tilde{c}^\dagger_{C\vec{k}} \tilde{c}_{D\vec{k}'} \tilde{c}^\dagger_{\epsilon_2} \tilde{c}_{\epsilon_1} |i\rangle, \tag{29}$$

where $\epsilon_2 \neq \epsilon_1$. In comparison with $|i\rangle$, $|f\rangle$ has one more electron in the reservoir C, one less electron in the reservoir D, and one more particle-hole excitation in the charge Kondo system. $W_i = e^{-E_i/(k_BT)}/Z$ is the probability of having the initial state $|i\rangle$, where Z is the partition function. Note that the processes described by H_{Pz} do not contribute to $\Gamma^{C\leftarrow D}$ in the lowest-order Fermi golden rule. The Fermi golden rule expression of $\Gamma^{D\leftarrow C}$ has a similar form.

Each initial state $|i\rangle$ is further decomposed as $|i\rangle = |i_K\rangle|i_C\rangle|i_D\rangle$, where $|i_K\rangle$, $|i_C\rangle$ and $|i_D\rangle$ are eigenstates of H_{0K}, H_{0C}, and H_{0D}, respectively. Then, the transition rate $\Gamma^{C\leftarrow D}$ is obtained as

$$\begin{aligned}
\Gamma^{C\leftarrow D} &= 2\pi \sum_{\vec{k},\vec{k}',\epsilon_1,\epsilon_2} \sum_{|i\rangle} W_i |\langle i|\tilde{c}^\dagger_{\epsilon_1}\tilde{c}_{\epsilon_2}\tilde{c}^\dagger_{D\vec{k}'}\tilde{c}_{C\vec{k}} V_P \sum_{\vec{k}_1,\vec{k}_2,\vec{k}_3} \tilde{c}^\dagger_{C\vec{k}_3}\tilde{c}_{D\vec{k}_2}\tilde{c}^\dagger_{\vec{k}_1}\tilde{c}_d|i\rangle|^2 \delta(\epsilon_{\vec{k}} - \epsilon_{\vec{k}'} + \epsilon_2 - \epsilon_1) \\
&= 2\pi V_P^2 \sum_{\vec{k},\vec{k}',\epsilon_1,\epsilon_2} \sum_{|i\rangle=|i_C\rangle|i_D\rangle|i_K\rangle} |\langle i_D|\tilde{c}^\dagger_{D\vec{k}'}\tilde{c}_{D\vec{k}'}|i_D\rangle|^2 |\langle i_C|\tilde{c}_{C\vec{k}}\tilde{c}^\dagger_{C\vec{k}}|i_C\rangle|^2 |\langle i_K|\tilde{c}^\dagger_{\epsilon_1}\tilde{c}_{\epsilon_2}\sum_{\vec{k}_1}\tilde{c}^\dagger_{\vec{k}_1}\tilde{c}_d|i_K\rangle|^2 \\
&\quad \times W_i \delta(\epsilon_{\vec{k}} - \epsilon_{\vec{k}'} + \epsilon_2 - \epsilon_1) \\
&= 2\rho^3 V_P^2 \int d\epsilon_{\vec{k}} d\epsilon_{\vec{k}'} d\epsilon_1 d\epsilon_2 \frac{T_K}{T_K^2+\epsilon_1^2}\frac{\epsilon_2^2}{T_K^2+\epsilon_2^2} f_D(\epsilon_{\vec{k}'})(1-f_C(\epsilon_{\vec{k}}))f(\epsilon_1)(1-f(\epsilon_2))\delta(\epsilon_{\vec{k}} - \epsilon_{\vec{k}'} + \epsilon_2 - \epsilon_1).
\end{aligned} \tag{30}$$

In the above equation, we used the decomposition of

$$W_i = \frac{e^{-E_{i_K}/(k_BT)}}{Z_K}\frac{e^{-E_{i_C}/(k_BT)}}{Z_C}\frac{e^{-E_{i_D}/(k_BT)}}{Z_D}, \tag{31}$$

where Z_K, Z_C, and Z_D are the partition functions of H_{0K}, H_C, and H_D, respectively, and E_{i_K}, E_{i_C}, and E_{i_D} are the energies of states $|i_K\rangle$, $|i_C\rangle$, and $|i_D\rangle$. We also used the relation

$$\sum_{|i_C\rangle} |\langle i_C|\tilde{c}^\dagger_{C\vec{k}}\tilde{c}_{C\vec{k}}|i_C\rangle|^2 \frac{e^{-E_{i_C}/(k_BT)}}{Z_C} = f_C(\epsilon_{\vec{k}}) \tag{32}$$

for the reservoir C, and the equation (see Appendix for the derivation)

$$\begin{aligned}
&\sum_{|i_K\rangle} |\langle i_K|\tilde{c}^\dagger_{\epsilon_1}\tilde{c}_{\epsilon_2}\sum_{\vec{k}_1}\tilde{c}^\dagger_{\vec{k}_1}\tilde{c}_d|i_K\rangle|^2 \frac{e^{-E_{i_K}/(k_BT)}}{Z_K} \\
&\quad = \frac{1}{\pi\rho}\frac{T_K}{T_K^2+\epsilon_1^2}\frac{\epsilon_2^2}{T_K^2+\epsilon_2^2} f(\epsilon_1)(1-f(\epsilon_2)).
\end{aligned} \tag{33}$$

Using Eqs. (30) and (26), we obtain the zero-bias differential conductance dI_{CD}/dV_{CD} at temperature T and at $V_{CD}\to 0$,

$$\frac{dI_{CD}}{dV_{CD}} \propto \frac{e^2}{h}\frac{\rho J_{P+}^2}{T_K}\left(\frac{T}{T_K}\right)^2 (\rho T)^2, \tag{34}$$

where the expression of J_{P+} is found in Eq. (25). The temperature dependence of $dI_{CD}/dV_{CD} \propto T^4$ is different from the usual temperature dependence $\propto T^2$ [see, e.g., Eq. (20)]. It is because the conductance is induced by the electron tunneling t_1 (occurring between the dot C and the reservoir C and between the dot D and the reservoir D in the processes of H_{P+}) which is not described by the Kondo Hamiltonian H^{CNT}_{eff1} but by H_{P+} in Eq. (25). The factor $\rho J_{P+}^2/T_K$ ($\ll 1$ in the perturbation regime) is understood as the number of the pseudospin flips induced by the electron tunneling t_1 within the Kondo characteristic time $1/T_K$. The factor $(T/T_K)^2$ in Eq. (34) shows the usual Fermi-liquid behavior of $(T/T_K)^2$ and originates from electron tunneling between the quadruple dot and the reservoirs A and B in the processes of H_{P+}. The last factor $(\rho T)^2$ comes from the energy window of the reservoirs C and D available for the processes of H_{P+} at temperature T. The nontrivial temperature dependence of dI_{CD}/dV_{CD} will be useful for identifying the charge Kondo effects of the quadruple dot in the CNT setup. We note that the result in Eq. (34), obtained exactly at the Toulouse point, is valid also near the Toulouse point; when the system deviates perturbatively from the Toulouse point, the correction to Eq. (34) is of sixth order in temperature [see Eq. (A11) in Appendix].

We estimate the Kondo temperature T_K of the charge Kondo effect in the CNT quadruple dot, using Eq. (24). T_K can reach about 1.5 K with the parameters [54,61,62] of $V \sim$ 1–2 meV, $U_{AB} \sim$ 0.4–0.8 meV, $t_{CD} \sim$ 0.1–0.8 meV, and $\Gamma \sim$ 0.1–0.4 meV.

E. Asymmetry between the dots A and B

We study the stability of the charge Kondo effect against asymmetry between A and B. The asymmetry occurs when the single-particle level $\epsilon_A = \epsilon_0 + \delta\epsilon_A$ of the dot A is different from that $\epsilon_B = \epsilon_0 + \delta\epsilon_B$ of the dot B, $\delta\epsilon_A \neq \delta\epsilon_B$. This lifts the energy degeneracy of the pseudospin states $|\Uparrow\rangle$ and $|\Downarrow\rangle$, resulting in pseudospin Zeeman energy $E_{PZ} = \delta\epsilon_A + \delta\epsilon_B$. Be-

low, we compute the effect of the asymmetry on the electron current in the 2DEG setup [see Fig. 1(a)], considering the Fermi liquid regime of small asymmetry $\delta\epsilon_{\rm A}, \delta\epsilon_{\rm B} \ll k_B T_K$.

Applying the Schrieffer-Wolff transformation, we find that in the presence of the asymmetry, the effective Hamiltonian in Eq. (11) has the pseudospin Zeeman term $H_{\rm PZ}$ and the potential scattering $H_{\rm W}$,

$$\begin{aligned} H_{\rm eff1} &\to H_{\rm eff1} + H_{\rm PZ} + H_{\rm W}, \\ H_{\rm PZ} &= E_{\rm PZ}\tau_z, \\ H_{\rm W} &= \sum_{\lambda={\rm A,B};\vec{k},\vec{k}'} W_\lambda c^\dagger_{\lambda\vec{k}} c_{\lambda\vec{k}'}, \\ W_\lambda &= t_0^2\left[\frac{1}{\epsilon_0+V-\delta\epsilon_\lambda} - \frac{1}{\epsilon_0+V+\delta\epsilon_\lambda}\right] \approx \frac{2t_0^2\delta\epsilon_\lambda}{(\epsilon_0+V)^2}. \end{aligned} \tag{35}$$

The asymmetry leads to additional scattering phase shifts. The pseudospin Zeeman term $H_{\rm PZ}$ plays the same role [63] as the elastic scattering α term in Eq. (15). The potential scattering modifies the scattering phase $\delta_c(\epsilon) \to \delta_c(\epsilon) + \delta_{{\rm PS},\lambda}$ of electron transmission through dot $\lambda = {\rm A, B}$. $\delta_{{\rm PS},\lambda}$ can be obtained [64] as $\delta_{{\rm PS},\lambda} = -\arctan(\pi\rho W_\lambda)$, using the T matrix.

Combining these, we find the current $I_{\rm A}$ through the dot A,

$$\begin{aligned} I_{\rm A} = \frac{e^2}{h}\Bigg[& V_{\rm A}\cos^2(\delta_{\rm PS,A}) - \frac{V_{\rm A}}{4}\cos(2\delta_{\rm PS,A}) \\ & \times\left\{\left(\frac{eV_{\rm A}}{k_BT_K}\right)^2 + \left(\frac{eV_{\rm B}}{k_BT_K}\right)^2 + \left(\frac{E_{\rm PZ}}{k_BT_K}\right)^2\right\}\Bigg]. \end{aligned} \tag{36}$$

The result becomes identical to Eq. (19) in the limit of $E_{\rm PZ} = 0$ and $\delta\epsilon_\lambda = 0$.

IV. ANISOTROPIC TWO-CHANNEL CHARGE KONDO EFFECTS IN THE SPINFUL REGIME

We next move to the spinful regime of $t_{\rm AB} \neq 0$ and $E_{\rm Z} = 0$. We will show that a two-channel charge Kondo Hamiltonian describes the quadruple dot when (i) ($n_{\rm A} = 1, n_{\rm B} = 1, n_{\rm C} = 1, n_{\rm D} = 0$) and (0,0,0,1) are the degenerate ground-state charge configurations and (ii) the (1,1,1,0) configuration has a spin-singlet state in the subsystem AB. The two-channel Kondo Hamiltonian has channel anisotropy due to interdot electron tunneling. Because of the anisotropy, the single-channel charge Kondo effect, induced from the two-channel Hamiltonian, appears in the parameter regime available in current experiments.

A. Parameter regime and pseudospin

When the quadruple dot has the charge configuration ($n_{\rm A} = 1, n_{\rm B} = 1, n_{\rm C} = 1, n_{\rm D} = 0$), the subsystem AB has two electrons. The two electrons form a spin singlet, since electron tunneling occurs between the dots A and B ($t_{\rm AB} \neq 0$) and there is no external magnetic field ($E_{\rm Z} = 0$); the tunneling causes antiferromagnetic coupling between A and B with coupling strength $J_{\rm AB} = \frac{4t_{\rm AB}^2}{U-U_{\rm AB}}$. The ground state is $\frac{1}{\sqrt{2}}(d^\dagger_{{\rm A}\uparrow}d^\dagger_{{\rm B}\downarrow} - d^\dagger_{{\rm A}\downarrow}d^\dagger_{{\rm B}\uparrow})d^\dagger_{\rm C}|0\rangle$ and has energy $2\epsilon_0 + U_{\rm AB} - J_{\rm AB} + \epsilon_{\rm C}$. On the other hand, the state of the charge configuration (0,0,0,1) is

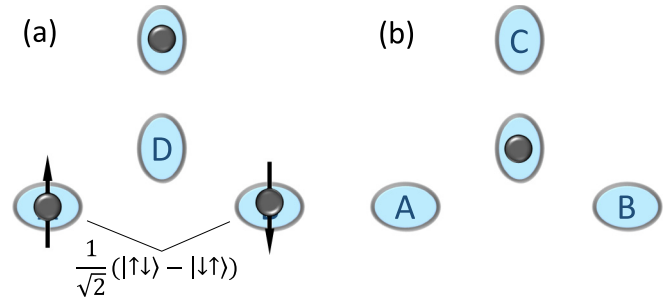

FIG. 4. Pseudospins of the quadruple dot in the spinful regime of $E_{\rm Z} = 0$ and $t_{\rm AB} \neq 0$. (a) The charge configuration (1,1,1,0) having the spin singlet $\frac{1}{\sqrt{2}}(d^\dagger_{{\rm A}\uparrow}d^\dagger_{{\rm B}\downarrow} - d^\dagger_{{\rm A}\downarrow}d^\dagger_{{\rm B}\uparrow})d^\dagger_C|0\rangle$ in the subsystem AB corresponds to the pseudospin up. (b) The configuration (0,0,0,1) corresponds to the pseudospin down.

$d^\dagger_{\rm D}|0\rangle$ and has energy $\epsilon_{\rm D}$. The conditions for the two states

$$|\Uparrow'\rangle = \frac{1}{\sqrt{2}}(d^\dagger_{{\rm A}\uparrow}d^\dagger_{{\rm B}\downarrow} - d^\dagger_{{\rm A}\downarrow}d^\dagger_{{\rm B}\uparrow})d^\dagger_{\rm C}|0\rangle, \quad |\Downarrow'\rangle = d^\dagger_{\rm D}|0\rangle \tag{37}$$

to form the degenerate ground states are (i) $\epsilon_{\rm D} = 2\epsilon_0 + U_{\rm AB} - J_{\rm AB} + \epsilon_{\rm C}$ (with which the two states have the same energy), (ii) $0 < \epsilon_{\rm C} - \epsilon_{\rm D} < 2V$ and $-V < \epsilon_0 < J_{\rm AB} - U_{\rm AB}$ [with which the two states are the ground states, having lower energy than the other states such as $d^\dagger_{{\rm A}\uparrow}d^\dagger_{\rm C}|0\rangle$ and $\frac{1}{\sqrt{2}}(d^\dagger_{{\rm A}\uparrow}d^\dagger_{{\rm B}\downarrow} - d^\dagger_{{\rm A}\downarrow}d^\dagger_{{\rm B}\uparrow})d^\dagger_{\rm D}|0\rangle$].

We ignore the ordinary spin Kondo effect in each of the dots A and B, considering [65] that $J_{\rm AB}$ is much larger than the Kondo temperature of the spin Kondo effect, and the energy difference between the ground states and excited states must be larger than the single-particle level broadening Γ and the thermal energy, for example, $J_{\rm AB} > \Gamma$.

Note that we ignore the spin degrees of freedom of electrons in the dots C and D, since there is no electron tunneling between the subsystems CD and AB. We also choose the condition of $\epsilon_{\rm D} + V = \epsilon_{\rm C}$ for computational convenience, as in Sec. III A; relaxation of these conditions do not alter our results qualitatively.

The two degenerate ground states $|\Uparrow'\rangle$ and $|\Downarrow'\rangle$ form the pseudospin up and down (see Fig. 4). The pseudospin-1/2 operators are $S_z = (|\Uparrow'\rangle\langle\Uparrow'| - |\Downarrow'\rangle\langle\Downarrow'|)/2$, $S_+ = |\Uparrow'\rangle\langle\Downarrow'|$, and $S_- = |\Downarrow'\rangle\langle\Uparrow'|$.

B. Two-channel Kondo effect

Under the above conditions, we obtain a low-energy effective Hamiltonian in terms of the pseudospin operators, by applying the Schrieffer-Wolff transformation [55],

$$H_{\rm eff2} = H_{\rm A\|B} + H_{\rm A\leftrightarrow B} + H_{\rm res}. \tag{38}$$

The Hamiltonian $H_{\rm eff2}$ for the coupling between the pseudospin operators and the reservoir electrons is decomposed into the two terms, $H_{\rm A\|B}$ and $H_{\rm A\leftrightarrow B}$. $H_{\rm A\|B}$ is

$$\begin{aligned} H_{\rm A\|B} = & \sum_{\vec{k},\vec{k}';\lambda={\rm A,B}} J_{1z}S_z(c^\dagger_{\lambda\vec{k}\uparrow}c_{\lambda\vec{k}'\uparrow} + c^\dagger_{\lambda\vec{k}\downarrow}c_{\lambda\vec{k}'\downarrow}) \\ & + \sum_{\vec{k},\vec{k}'} J_{1+}S_+(c_{{\rm A}\vec{k}\downarrow}c_{{\rm B}\vec{k}'\uparrow} + c_{{\rm B}\vec{k}\downarrow}c_{{\rm A}\vec{k}'\uparrow}) + {\rm H.c.} \end{aligned}$$

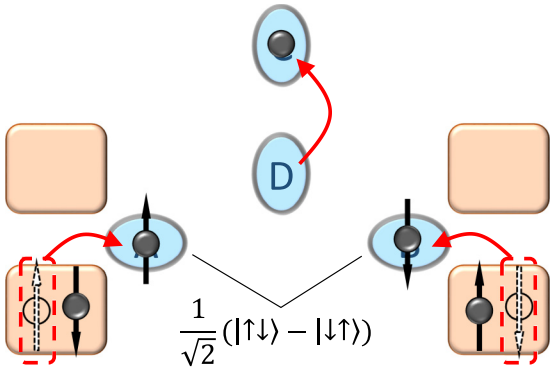

FIG. 5. A process contributing to the J_{1+} term of $H_{\mathrm{A}\|\mathrm{B}}$. It results in pseudospin flip from $|\Downarrow'\rangle = d_{\mathrm{D}}^{\dagger}|0\rangle$ to $|\Uparrow'\rangle = \frac{1}{\sqrt{2}}(d_{\mathrm{A}\uparrow}^{\dagger} d_{\mathrm{B}\downarrow}^{\dagger} - d_{\mathrm{A}\downarrow}^{\dagger} d_{\mathrm{B}\uparrow}^{\dagger}) d_{\mathrm{C}}^{\dagger}|0\rangle$. The process has three electron-tunneling events (red arrows), tunneling of a spin-up electron from the reservoir ηA to the dot A, tunneling of a spin-down electron from the reservoir ηB to the dot B, and tunneling of an electron from the dot D to the dot C. There is another process (not shown in this figure) contributing to the J_{1+} term. It is composed of tunneling of a spin-down electron from ηA to A, tunneling of a spin-up electron from ηB to B, and tunneling of an electron from D to C.

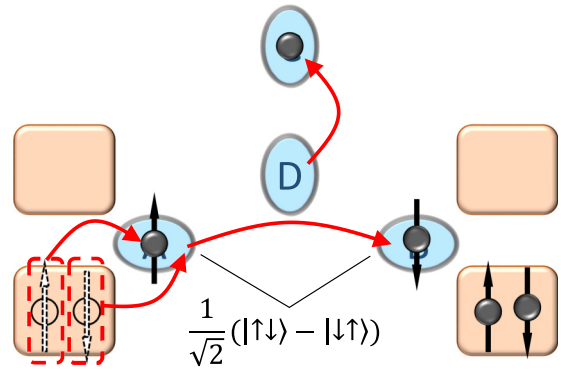

FIG. 6. A process contributing to the J_{2+} term of $H_{\mathrm{A}\leftrightarrow\mathrm{B}}$. It results in pseudospin flip from $|\Downarrow'\rangle$ to $|\Uparrow'\rangle$. It has four electron-tunneling events (red arrows), tunneling of a spin-up electron from the reservoir ηA to the dot A, tunneling of a spin-down electron from the reservoir ηA to the dot A, followed by tunneling of the spin-down electron from the dot A to the dot B, and tunneling of an electron from the dot D to the dot C. There are other processes (not shown in this figure) contributing to the J_{2+} term. For example, there is a process composed of tunneling of a spin-down electron from ηA to A, tunneling of a spin-up electron from ηA to A, followed by tunneling of the spin-up electron from A to B, and tunneling of an electron from D to C.

$$+ \sum_{\vec{k},\vec{k}';\lambda=\mathrm{A,B}} W_1 (c_{\lambda\vec{k}\uparrow}^{\dagger} c_{\lambda\vec{k}'\uparrow} + c_{\lambda\vec{k}\downarrow}^{\dagger} c_{\lambda\vec{k}'\downarrow}),$$

$$J_{1z} = \frac{3t_0^2}{\epsilon_0 + V}, \qquad W_1 = -\frac{t_0^2}{2(\epsilon_0 + V)}$$

$$J_{1+} = -\frac{2\sqrt{2}t_0^2 t_{\mathrm{CD}}}{\epsilon_0 + V}\left[\frac{2}{V} + \frac{1}{\epsilon_0 + V}\right]. \tag{39}$$

$H_{\mathrm{A}\|\mathrm{B}}$ results from processes not involving interdot electron tunneling between the dots A and B. It has pseudospin nonflip terms of strength J_{1z}, pseudospin flip terms of J_{1+}, and potential scattering of W_1. An example of the processes is illustrated in Fig. 5.

Next, $H_{\mathrm{A}\leftrightarrow\mathrm{B}}$ results from processes involving interdot tunneling between the dots A and B.

$$H_{\mathrm{A}\leftrightarrow\mathrm{B}} = \sum_{\vec{k},\vec{k}';\sigma=\uparrow,\downarrow} J_{2z} S_z (c_{\mathrm{A}\vec{k}\sigma}^{\dagger} c_{\mathrm{B}\vec{k}'\sigma} + c_{\mathrm{B}\vec{k}\sigma}^{\dagger} c_{\mathrm{A}\vec{k}'\sigma})$$

$$+ \sum_{\vec{k},\vec{k}',\lambda=\mathrm{A,B}} J_{2+} S_+ c_{\lambda\vec{k}\downarrow} c_{\lambda\vec{k}'\uparrow} + \mathrm{H.c.}$$

$$+ \sum_{\vec{k},\vec{k}',\sigma=\uparrow,\downarrow} W_2 (c_{\mathrm{A}\vec{k}\sigma}^{\dagger} c_{\mathrm{B}\vec{k}'\sigma} + c_{\mathrm{B}\vec{k}\sigma}^{\dagger} c_{\mathrm{A}\vec{k}'\sigma}),$$

$$J_{2z} = -\frac{3t_0^2 t_{\mathrm{AB}}}{(\epsilon_0 + V)^2}, \qquad W_2 = \frac{t_0^2 t_{\mathrm{AB}}}{2(\epsilon_0 + V)^2}$$

$$J_{2+} = \frac{2\sqrt{2}t_0^2 t_{\mathrm{CD}} t_{\mathrm{AB}}}{(\epsilon_0 + V)^2}\left[\frac{2}{V} + \frac{2}{\epsilon_0 + V}\right]. \tag{40}$$

Because of interdot tunneling between A and B, the coupling energies J_{2z}, J_{2+}, W_2 of $H_{\mathrm{A}\leftrightarrow\mathrm{B}}$ are smaller than those of $H_{\mathrm{A}\|\mathrm{B}}$: $J_{2z} = -J_{1z} t_{\mathrm{AB}}/(\epsilon_0 + V)$, $J_{2+} = -J_{1+} t_{\mathrm{AB}}(2\epsilon_0 + 4V)/(\epsilon_0 + V)(2\epsilon_0 + 3V)$, $W_2 = -W_1 t_{\mathrm{AB}}/(\epsilon_0 + V)$. An example of the processes leading to $H_{\mathrm{A}\leftrightarrow\mathrm{B}}$ is illustrated in Fig. 6.

In this spinful regime of $E_{\mathrm{Z}} = 0$ and $t_{\mathrm{AB}} \neq 0$, both of the charge and spin degrees of freedom are important, as shown in Eq. (38), and they can result in a two-channel Kondo effect, contrary to the spinless regime of $E_{\mathrm{Z}} \gg U_{\lambda\lambda'}$ and $t_{\mathrm{AB}} = 0$ studied in Sec. III. To understand how H_{eff2} in Eq. (38) describes the two-channel Kondo effect, we first consider $H_{\mathrm{A}\|\mathrm{B}} + H_{\mathrm{res}}$, a part of H_{eff2}. In $H_{\mathrm{A}\|\mathrm{B}}$, the pseudospin flip $|\Uparrow'\rangle \leftrightarrow |\Downarrow'\rangle$ occurs in two ways that behave as two independent channels, (i) tunneling of a spin-up electron between the dot A and the reservoirs ηA and tunneling of a spin-down electron between the dot B and the reservoirs ηB (see Fig. 5) and (ii) tunneling of a spin-down electron between A and ηA and tunneling of a spin-up electron between B and ηB. To see this, we rewrite $H_{\mathrm{A}\|\mathrm{B}} + H_{\mathrm{res}}$, applying the particle-hole transformation of $c_{\mathrm{A(B)}\vec{k}\downarrow} \to c_{\mathrm{A(B)}\vec{k}\downarrow}^{\dagger}$ and $\epsilon_{\eta\mathrm{A(B)}\vec{k}\downarrow} \to -\epsilon_{\eta\mathrm{A(B)}\vec{k}\downarrow}$, and assigning pseudospin up and channel index $(\Uparrow, \mathrm{ch} = 1)$ to ηA $\uparrow$ electrons, $(\Downarrow, \mathrm{ch} = 1)$ to ηB $\downarrow$, $(\Uparrow, \mathrm{ch} = 2)$ to ηB $\uparrow$, and $(\Downarrow, \mathrm{ch} = 2)$ to ηA $\downarrow$,

$$H_{\mathrm{A}\|\mathrm{B}} + H_{\mathrm{res}} \to \sum_{\mathrm{ch}=1,2} 2J_{1z} S_z s_z^{\mathrm{ch}} + J_{1+} S_+ s_-^{\mathrm{ch}} + \mathrm{H.c.}$$

$$+ \sum_{\mathrm{ch}=1,2} W_1 (c_{\mathrm{ch},\vec{k}\Uparrow}^{\dagger} c_{\mathrm{ch},\vec{k}'\Uparrow} - c_{\mathrm{ch},\vec{k}\Downarrow}^{\dagger} c_{\mathrm{ch},\vec{k}'\Downarrow})$$

$$+ H_{\mathrm{res}}. \tag{41}$$

Here, $s_{i=x,y,z}^{\mathrm{ch}=1,2} = \sum_{\vec{k}\vec{k}';\mu\mu'=\Uparrow,\Downarrow} c_{\mathrm{ch},\vec{k}\mu}^{\dagger} \frac{\sigma_{\mu\mu'}^{i}}{2} c_{\mathrm{ch},\vec{k}'\mu'}$ and $s_{\pm}^{\mathrm{ch}} = s_x^{\mathrm{ch}} \pm i s_y^{\mathrm{ch}}$. This shows that $H_{\mathrm{A}\|\mathrm{B}} + H_{\mathrm{res}}$ describes a two-channel charge Kondo effect. The two-channel Kondo Hamiltonian in Eq. (41) has channel isotropy, namely, the coupling strengths J_{1z}, J_{1+}, and W_1 are independent of the channel index.

Therefore, it shows a two-channel Kondo effect at zero temperature. Note that the Kondo effect has spin anisotropy, $J_{1+} \neq J_{1z}$, as in the single-channel Kondo effect in the spinless regime of $E_Z \gg U_{\lambda\lambda'}$ and $t_{AB} = 0$ [see the Hamiltonian in Eq. (11)].

Now we discuss the effect of $H_{A\leftrightarrow B}$ on the two-channel Kondo effect. In this Hamiltonian, tunneling of two electrons (one having up real spin, and the other having down real spin) from a reservoir (e.g., the reservoir SA in Fig. 6) to the subsystem AB can result in the pseudospin flip $|\Uparrow'\rangle \leftrightarrow |\Downarrow'\rangle$, contrary to the case of $H_{A\|B}$; in the case of $H_{A\|B}$, the pseudospin flip occurs only by tunneling of two electrons, one from the reservoir ηA and the other from the reservoir η'B (see Fig. 5). This effect of $H_{A\leftrightarrow B}$ can suppress the two-channel Kondo effect of $H_{A\|B} + H_{res}$. To see this, we apply the particle-hole transformation of $c_{A(B)\vec{k}\downarrow} \to c^\dagger_{A(B)\vec{k}\downarrow}$ and $\epsilon_{\eta A(B)\vec{k}\downarrow} \to -\epsilon_{\eta A(B)\vec{k}\downarrow}$ (which was used for $H_{A\|B}$) to $H_{A\leftrightarrow B}$, and introduce the even and odd combinations of the channels for each pseudospin $\mu = \Uparrow, \Downarrow$,

$$c_{\mathrm{ch}=e,\vec{k}\mu} = \frac{1}{\sqrt{2}}(c_{\mathrm{ch}=1,\vec{k}\mu} + c_{\mathrm{ch}=2,\vec{k}\mu}),$$
$$c_{\mathrm{ch}=o,\vec{k}\mu} = \frac{1}{\sqrt{2}}(c_{\mathrm{ch}=1,\vec{k}\mu} - c_{\mathrm{ch}=2,\vec{k}\mu}). \quad (42)$$

Then, the total Hamiltonian $H_{\mathrm{eff}2} = H_{A\|B} + H_{A\leftrightarrow B} + H_{res}$ in Eq. (38) is written as

$$H_{2ch} = H_{res} + \sum_{\mathrm{ch}=e,o} 2J_z^{ch} S_z s_z^{ch} + J_+^{ch} S_+ s_+^{ch} + \mathrm{H.c.}$$
$$+ \sum_{\vec{k},\vec{k}'} \sum_{\mathrm{ch}=e,o} W^{ch}(c^\dagger_{ch,\vec{k}\Uparrow} c_{ch,\vec{k}'\Uparrow} - c^\dagger_{ch,\vec{k}\Downarrow} c_{ch,\vec{k}'\Downarrow}), \quad (43)$$

where the coupling strengths are $J_z^{ch=e} = (J_{1z} + J_{2z})/2$, $J_z^{ch=o} = (J_{1z} - J_{2z})/2$, $J_+^{ch=e} = (J_{1+} + J_{2+})/2$, $J_+^{ch=o} = (J_{1+} - J_{2+})/2$, $W^{ch=e} = (W_1 + W_2)/2$, and $W^{ch=o} = (W_1 - W_2)/2$. This Hamiltonian describes a two-channel charge Kondo effect with the two independent screening channels shown in Eq. (42). The pseudospin flip $|\Uparrow'\rangle \leftrightarrow |\Downarrow'\rangle$ occurs by tunneling of two even-channel electrons or independently by two odd-channel electrons. The even-odd channel combinations in Eq. (42) are related to the A-B symmetry between the A side (the dot A and its reservoirs ηA) and the B side (B and ηB). When the symmetry is relaxed, there appear two linear combinations of the channels ch $= 1, 2$ that independently screen the impurity spin states $|\Uparrow'\rangle$ and $|\Downarrow'\rangle$.

We notice that the Hamiltonian H_{2ch} in Eq. (43) has channel anisotropy $J_{z,+}^{ch=e} > J_{z,+}^{ch=o}$ and spin anisotropy $J_z^{ch=e,o} > J_+^{ch=e,o}$. The channel anisotropy originates from electron tunneling t_{AB} between the dots A and B. The channel anisotropy weakens the two-channel Kondo effect, as discussed later.

The channel anisotropy is unavoidable. To make the two-channel Kondo Hamiltonian H_{2ch} more isotropic, one may reduce the strength t_{AB} of interdot electron tunneling between A and B, the origin of the channel anisotropy. In this case, however, the energy gap between the spin singlet [which forms the pseudospin state $|\Uparrow'\rangle$ in Eq. (37)] and the spin triplets of the subsystem AB becomes smaller, which weakens the two-channel charge Kondo effect.

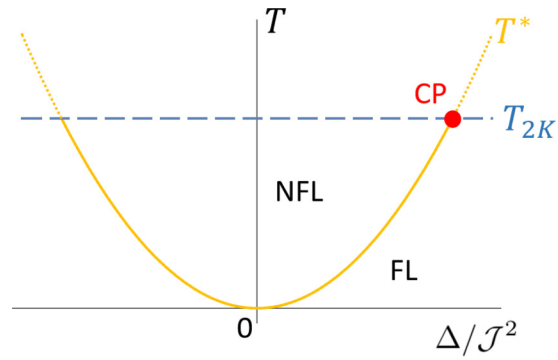

FIG. 7. Schematic phase diagram of a two-channel Kondo effect as a function of temperature T and channel anisotropy Δ. $\mathcal{J}$ is a dimensionless coupling strength (see the text). Two crossover temperatures T_{2K} (blue dashed curve) and T^* (orange solid) exist, depending on Δ. When $T^* < T_{2K}$, a single-channel Kondo effect and its Fermi liquid (FL) appear at $T \lesssim T^*$, the two-channel Kondo effect and its non-Fermi liquid (NFL) occur at $T^* \lesssim T \lesssim T_{2K}$, and the two-channel Kondo effect becomes suppressed at higher temperature. When $T^* > T_{2K}$ [the right side of the crossing point (CP) of T_{2K} and T^*], a single-channel Kondo effect occurs at temperature lower than the single-channel Kondo temperature.

C. Channel anisotropy

When there is channel anisotropy in a two-channel Kondo Hamiltonian, there are two crossover temperatures T^* and T_{2K} [66,67]. Then, depending on temperature T and the anisotropy, there occurs a two-channel Kondo effect or a single-channel Kondo effect, as sketched in Fig. 7. Below, we estimate T^* and T_{2K} of the two-channel Kondo Hamiltonian in Eq. (43).

In order to estimate the two crossover temperatures, we apply the Poorman's scaling [56,68]. We introduce dimensionless average coupling strengths $\mathcal{J}_z$ and $\mathcal{J}_+$, and dimensionless channel anisotropies Δ_z and Δ_+,

$$\mathcal{J}_z \equiv \rho\big(J_z^{ch=e} + J_z^{ch=o}\big)/2 = \rho J_{1z}/2,$$
$$\Delta_z \equiv \rho(J_z^{ch=e} - J_z^{ch=o}) = \rho J_{2z},$$
$$\mathcal{J}_+ \equiv \rho(J_+^{ch=e} + J_+^{ch=o})/2 = \rho J_{1+}/2,$$
$$\Delta_+ \equiv \rho(J_+^{ch=e} - J_+^{ch=o}) = \rho J_{2+}, \quad (44)$$

where ρ is the density of states of the reservoirs. We obtain the coupled scaling equations,

$$\frac{d\mathcal{J}_z}{d\ln D} = -\frac{1}{2}\Delta_+^2 - 2\mathcal{J}_+^2,$$
$$\frac{d\Delta_z}{d\ln D} = -4\Delta_+\mathcal{J}_+,$$
$$\frac{d\mathcal{J}_+}{d\ln D} = -\left(2\mathcal{J}_z\mathcal{J}_+ + \frac{1}{2}\Delta_z\Delta_+\right),$$
$$\frac{d\Delta_+}{d\ln D} = -2(\Delta_z\mathcal{J}_+ + \mathcal{J}_z\Delta_+), \quad (45)$$

where D is the effective bandwidth of the reservoirs.

To estimate T^* and T_{2K}, we consider the case [68] of $\mathcal{J} = \mathcal{J}_z \simeq \mathcal{J}_+$, $\Delta = \Delta_z \simeq \Delta_+$, and $\Delta \ll \mathcal{J}$. T_{2K} is estimated as $T_{2K} \sim D_0 \exp[-1/2\mathcal{J}(D_0)]$, which is the effective bandwidth D at the point of $\mathcal{J} \sim 1$ in the renormalization group flow of the scaling equations. Here D_0 is the bare bandwidth of the reservoirs. T^* is estimated by the effective bandwidth D at the point of $\Delta \sim 1$. Using Eqs. (39), (40), (45) and the fact [66] that the scaling dimension of the channel anisotropy is 1/2, we have the relation between T^* and T_{2K},

$$\frac{T^*}{T_{2K}} \sim \left(\frac{\Delta}{\mathcal{J}^2}\right)^2 \sim 16\frac{J_{2z}^2}{\rho^2 J_{1z}^4} \sim 4\frac{t_{\rm AB}^2}{\Gamma^2}. \tag{46}$$

In the realistic situations of the setups in a 2DEG or CNTs, it is hard to satisfy simultaneously the condition $J_{\rm AB} > \Gamma$ (with which the spin singlet of the subsystem AB has lower energy than excited states by more than the single-particle level broadening Γ) and the condition of $T^* < T_{2K}$ (to have the temperature window for the two-channel Kondo effect). The former condition is equivalent with $4t_{\rm AB}^2/(U - U_{\rm AB}) > \Gamma$ and the latter $4t_{\rm AB}^2 < \Gamma^2$. The two conditions are simultaneously satisfied when $U - U_{\rm AB} < \Gamma$, which is however opposite to the Coulomb blockade condition of $U - U_{\rm AB} > \Gamma$. This implies $T^* > T_{2K}$, hence there occurs a single-channel Kondo effect induced from the two-channel Kondo Hamiltonian $H_{\rm 2ch}$.

In the single-channel charge Kondo effect, the pseudospin in Fig. 4 is screened by the even-parity channel $c^\dagger_{{\rm ch}=e}$ in Eq. (42), since the even-parity channel has stronger coupling than the odd-parity channel, $J_{z,+}^{{\rm ch}=e} > J_{z,+}^{{\rm ch}=o}$. By substituting $J_{ez}(J_{e+})$ into $J_z(J_+)$ in Eq. (24), we estimate the Kondo temperature T_{1K} of the single-channel Kondo effect, $T_{1K} \sim$ 20 mK for a quadruple dot formed in a 2DEG, based on $t_{\rm AB} \sim$ 40–70 μeV and the other parameters in Sec. III B, and $T_{1K} \sim 1$ K for a quadruple dot in CNTs, based on $t_{\rm AB} \sim$ 0.3–0.6 meV.

D. Electron transport

As discussed above, the single-channel charge Kondo effect by the even-parity channel occurs in the spinful regime, because of the large channel anisotropy. We compute the resulting electron transport through the quadruple quantum dot, applying the Fermi liquid theory in Sec. III C to the even-parity channel.

We first consider the setup of Fig. 1(a) at zero temperature. When bias voltage $V_{\rm SD}/2$ ($-V_{\rm SD}/2$) is applied to both the source reservoirs SA and SB (the drains DA and DB) and $V_{\rm SD}/2 \ll T_{1K}$, the electron current of the even-parity channel from the source reservoirs to the drain reservoirs DA and DB is found as

$$I_e = \frac{2e^2}{h}V_{\rm SD}\left[\cos^2(\delta_{{\rm p}e}) - \cos(2\delta_{{\rm p}e})\frac{1}{2}\left(\frac{eV_{\rm SD}}{k_B T_{1K}}\right)^2\right], \tag{47}$$

and the electron current of the odd-parity channel is obtained as $I_o = \frac{2e^2}{h}V_{\rm SD}\sin^2(\delta_{{\rm p}o})$, where $\delta_{{\rm p}e(o)} = -\arctan(\pi\rho W^{{\rm ch}=e(o)})$ comes from the potential scattering in Eq. (43). Then in the case that the quadruple dot has the A-B symmetry, the current $I_{\rm A(B)}$ detected at the drain DA (DB) is obtained as $I_{\rm A} = I_{\rm B} = (I_e + I_o)/2$. We find

$$I_{\rm A} = \frac{e^2}{h}V_{\rm SD}\left[\cos^2(\delta_{{\rm p}e}) + \sin^2(\delta_{{\rm p}o}) - \cos(2\delta_{{\rm p}e})\frac{1}{2}\left(\frac{eV_{\rm SD}}{k_B T_{1K}}\right)^2\right]. \tag{48}$$

Next we consider temperature larger than Kondo temperature ($T \gg T_{1K}$). Similarly to Eq. (23), we compute the conductance $dI_{\rm A}/dV_{\rm SD}$ in this temperature regime,

$$\frac{dI_{\rm A}}{dV_{\rm SD}} = \frac{e^2\pi^2\rho^2}{4h}\left(J_\Delta^e\right)^2\left[3\left(\frac{(1+(T/T_{1K})^{-4\rho J_\Delta^e})}{(1-(T/T_{1K})^{-4\rho J_\Delta^e})}\right)^2 - 2\right], \tag{49}$$

where $J_\Delta^e \equiv \sqrt{(J_z^{{\rm ch}=e})^2 - (J_+^{{\rm ch}=e})^2}$.

V. DISCUSSION AND SUMMARY

We have studied a quadruple quantum dot in the spinless and spinful regimes, when the system has twofold degenerate ground states of (1,1,1,0) and (0,0,0,1) charge configurations. In both the regimes, the quadruple dot exhibits the single-channel charge Kondo effect at low temperature that coherent fluctuations massively occur between the two charge configurations (1,1,1,0) and (0,0,0,1) with the help of electron tunneling between the quadruple dot and reservoirs. The charge Kondo effect has a similar origin to that of the negative-U Anderson impurity, as the electron interaction between the dots A and B is effectively attractive, although the bare interaction is repulsive, because of the repulsive Coulomb interaction between the subsystems AB and CD. We identified the impurity pseudospin states of the Kondo effect as well as the channel of conduction electrons screening the impurity pseudospin and obtained analytic expressions of electron current through the dot A in both the regimes. We also compared the charge Kondo effect with that of a triple quantum dot and analyzed the stability of the charge Kondo effect against pseudospin Zeeman effects. We expect that the single-channel charge Kondo effect appears in the realistic situations of a quadruple quantum dot in Fig. 1.

In the spinful regime of $t_{\rm AB} \neq 0$ and $E_{\rm Z} = 0$, a spin singlet is formed in the subsystem AB in the charge configuration (1,1,1,0). Interestingly, the low-energy properties of the quadruple quantum dot are described by a two-channel Kondo Hamiltonian with channel anisotropy. The channel anisotropy is unavoidable in realistic situations, and the quadruple dot shows a single-channel charge Kondo effect also in the spinful regime.

We briefly discuss the regimes not investigated in this work. In the regime of no external magnetic field ($E_{\rm Z} = 0$) and no interdot electron tunneling ($t_{\rm AB} = 0$) between the dots A and B, the spin degree of freedom plays a role. Due to the spin degree of freedom of subsystem AB, there are four different spin states for the (1,1,1,0) charge configuration. Then the charge Kondo effect will be suppressed, since there are five different degenerate ground states and the pseudospins of the

Kondo effect are not well defined. Instead, the ordinary spin Kondo effect occurs in each of the individual dots A and B. On the other hand, in the regime of an external magnetic field ($E_Z \neq 0$) and finite interdot electron tunneling ($t_{AB} \neq 0$), the single-channel charge Kondo effect of the spinless regime can appear when $E_Z > |\epsilon_0 + U_{AB}|, |\epsilon_0 + V| > |t_{AB}|$, or the single-channel Kondo effect of the spinful regime can occur when $J_{AB} > E_Z$. This work implies that charge Kondo effects and effective attractive interactions can appear in general multiple quantum dots when the multiple dots have two different ground-state charge configurations.

Note added. Recently, we became aware of a related contribution [69] on a charge Kondo effect of a quadruple quantum dot. This contribution and our work are complementary. In Ref. [69], the spinless regime of $t_{AB} = 0$ and large E_Z was studied using the numerical renormalization group method. In our work, we study both the spineless regime and the spinful regime of $t_{AB} \neq 0$ and $E_Z = 0$ and computed electron transports in the two regimes using the Fermi liquid theory. We also find that in the spinful regime, a single-channel charge Kondo effect is induced from a two-channel charge Kondo effect with large channel anisotropy. The overlap between the contribution and our work is only the result in Sec. III B.

ACKNOWLEDGMENT

This work is supported by Korea NRF (Grant No. 2016R1A5A1008184).

APPENDIX: DERIVATION OF EQ. (27)

In this Appendix, we derive the Hamiltonian in Eq. (27), applying the bosonization and refermionization method [60] to the single-channel Kondo Hamiltonian of the CNT setup in Eq. (25). We also discuss useful properties of the Hamiltonian.

In the bosonization, the electron density operator at position x of reservoir λ is written in terms of a boson field $\phi_\lambda(x)$ as

$$\psi_\lambda^\dagger(x)\psi_\lambda(x) = \partial_x\phi_\lambda(x) + \frac{2\pi\mathcal{N}_\lambda}{L}, \tag{A1}$$

and the field operator $\psi_\lambda(x=0)$ at position $x=0$ is

$$\psi_\lambda(x=0) = \sqrt{\frac{2\pi}{L}}\sum_{\vec{k}}\tilde{c}_{\lambda\vec{k}} = \frac{1}{\sqrt{a}}F_\lambda e^{-i\phi_\lambda(0)}. \tag{A2}$$

Here each reservoir is modeled as a one-dimensional system of length L, and it couples to the quadruple dot at $x=0$. $\mathcal{N}_\lambda \equiv \sum_{\vec{k}}\tilde{c}^\dagger_{\lambda\vec{k}}\tilde{c}_{\lambda\vec{k}}$ is the total number operator of electrons in reservoir λ, F_λ is the Klein factor of reservoir λ, and a is the short-distance cutoff.

Using the bosonic field $\phi_\lambda(x)$, the Kondo Hamiltonian of the CNT setup in Eq. (25) is written as

$$\begin{aligned}
H_{CNT} = H_{res}^{CNT} &+ \frac{L}{2\pi}J_z\sum_{\lambda=A,B}\tau_z\left[\partial\phi_\lambda(0) + \frac{2\pi\mathcal{N}_\lambda}{L}\right] \\
&+ J_+\left(\frac{L}{2\pi a}\right)\tau_+F_BF_Ae^{-i\phi_B(0)}F_Ae^{-i\phi_A(0)} \\
&+ \frac{L}{2\pi}J_{Pz}\tau_z\left[\partial\phi_C(0) - \partial\phi_D(0) + \frac{2\pi(\mathcal{N}_C-\mathcal{N}_D)}{L}\right] \\
&+ J_{P+}\left(\frac{L}{2\pi a}\right)^2\tau_+F_BF_Ae^{-i\phi_B(0)}F_Ae^{-i\phi_A(0)} \\
&\times F_D^\dagger e^{i\phi_D(0)}F_Ce^{-i\phi_C(0)}.
\end{aligned} \tag{A3}$$

Using the relations of

$$\begin{aligned}
\phi_{\tilde{c}/\tilde{s}}(x) &= (\phi_A(x) \pm \phi_B(x))/\sqrt{2} \\
\mathcal{N}_{\tilde{c}/\tilde{s}} &= (\mathcal{N}_A \pm \mathcal{N}_B)/2,
\end{aligned} \tag{A4}$$

we write the Hamiltonian as

$$\begin{aligned}
H_{CNT} = H_{res}^{CNT} &+ \sqrt{2}\frac{L}{2\pi}J_z\tau_z\left[\partial\phi_{\tilde{c}}(0) + \sqrt{2}\frac{2\pi\mathcal{N}_{\tilde{c}}}{L}\right] \\
&+ J_+\left(\frac{L}{2\pi a}\right)\tau_+F_BF_Ae^{-i\sqrt{2}\phi_{\tilde{c}}(0)} \\
&+ \frac{L}{2\pi}J_{Pz}\tau_z\left[\partial\phi_C(0) - \partial\phi_D(0) + \frac{2\pi(\mathcal{N}_C-\mathcal{N}_D)}{L}\right] \\
&+ J_{P+}\left(\frac{L}{2\pi a}\right)^2\tau_+F_BF_Ae^{-i\sqrt{2}\phi_{\tilde{c}}(0)} \\
&\times F_D^\dagger e^{i\phi_D(0)}F_Ce^{-i\phi_C(0)}.
\end{aligned} \tag{A5}$$

Then we apply the Emery-Kivelson transformation $U_1 = e^{i\gamma\tau_z\phi_{\tilde{c}}(0)}$ to the Hamiltonian at the so-called Toulouse point of $\sqrt{2}\frac{L}{2\pi}J_z = \gamma = \sqrt{2}-1$,

$$\begin{aligned}
H' =& U_1H_{CNT}U_1^\dagger \\
=& H_{res}^{CNT} + J_z\tau_z2\mathcal{N}_{\tilde{c}} + J_+\left(\frac{L}{2\pi a}\right)\tau_+F_BF_Ae^{-i\phi_{\tilde{c}}(0)} \\
&+ \frac{L}{2\pi}J_{Pz}\tau_z\left[\partial\phi_C(0) - \partial\phi_D(0) + \frac{2\pi(\mathcal{N}_C-\mathcal{N}_D)}{L}\right] \\
&+ J_{P+}\left(\frac{L}{2\pi a}\right)^2\tau_+F_BF_Ae^{-i\phi_{\tilde{c}}(0)}F_D^\dagger e^{i\phi_D(0)}F_Ce^{-i\phi_C(0)}.
\end{aligned} \tag{A6}$$

Then we apply the unitary operator $U_2 = e^{i\pi\mathcal{N}_{\tilde{c}}\tau_z}$ satisfying $U_2F_BF_AU_2^\dagger = e^{-i\pi\tau_z}F_BF_A$ and $U_2\tau_\pm U_2^\dagger = e^{\pm i\pi\mathcal{N}_{\tilde{c}}}\tau_\pm$, to obtain the refermionized Hamiltonian H_{EK} in Eq. (27)

$$\begin{aligned}
H_{EK} &= U_2H'U_2^\dagger \\
&= H_{0K} + H_{0C} + H_{0D} + H'_{Pz} + H'_{P+} + \text{constant}, \\
H_{0K} &= \sum_{\vec{k}}\epsilon_{\vec{k}}\tilde{c}^\dagger_{\vec{k}}\tilde{c}_{\vec{k}} + V_K\sum_{\vec{k}}(\tilde{c}^\dagger_d\tilde{c}_{\vec{k}} + \tilde{c}^\dagger_{\vec{k}}\tilde{c}_d), \\
H_{0C} &= \sum_{\vec{k}}\epsilon_{C\vec{k}}\tilde{c}^\dagger_{C\vec{k}}\tilde{c}_{C\vec{k}}, \qquad H_{0D} = \sum_{\vec{k}}\epsilon_{D\vec{k}}\tilde{c}^\dagger_{D\vec{k}}\tilde{c}_{D\vec{k}}, \\
H'_{Pz} &= \sum_{\vec{k},\vec{k}'}J_{Pz}(\tilde{c}^\dagger_d\tilde{c}_d - 1/2)(\tilde{c}^\dagger_{C\vec{k}}\tilde{c}_{C\vec{k}'} - \tilde{c}^\dagger_{D\vec{k}}\tilde{c}_{D\vec{k}'}), \\
H'_{P+} &= V_P\sum_{\vec{k}_1,\vec{k}_2,\vec{k}_3}\tilde{c}^\dagger_d\tilde{c}_{\vec{k}_1}\tilde{c}^\dagger_{D\vec{k}_2}\tilde{c}_{C\vec{k}_3} + \text{H.c.},
\end{aligned} \tag{A7}$$

where $V_K \equiv J_+\sqrt{L/2\pi a}$ and $V_P \equiv J_{P+}\sqrt{L/2\pi a}$. Here we used the pseudofermions of

$$\begin{aligned}\tilde{c}_d^\dagger &\equiv \tau_+ e^{i\pi(\mathcal{N}_{\tilde{c}}-\tau_z)}, \quad \tilde{c}_d^\dagger\tilde{c}_d = \tau_z + 1/2,\\ \psi_{\tilde{c}}(x) &\equiv \frac{F_{\rm B}F_{\rm A}}{\sqrt{a}} e^{-i\mathcal{N}_{\tilde{c}}2\pi x/L - i\phi_{\tilde{c}}(x)},\\ &\equiv \sqrt{2\pi/L}\sum_{\vec{k}} \tilde{c}_{\vec{k}} e^{-i\vec{k}x}. \end{aligned} \tag{A8}$$

Following Ref. [60], we diagonalize $H_{0K} = \sum_\epsilon \epsilon c_\epsilon^\dagger c_\epsilon$, using the unitary transformations of

$$\begin{aligned}\tilde{c}_d &= \sum_\epsilon \mathrm{Y}_\epsilon \tilde{c}_\epsilon, \qquad \mathrm{Y}_\epsilon = \left[\frac{T_K\Delta_L/\pi}{T_K^2 + (T_K\Delta_L/\pi) + \epsilon^2}\right]^{\frac{1}{2}},\\ \tilde{c}_{\vec{k}} &= \sum_\epsilon \mathrm{X}_{\vec{k}\epsilon}\tilde{c}_\epsilon, \qquad \mathrm{X}_{\vec{k}\epsilon} = \sqrt{\Delta_L T_K/\pi}\,\frac{1}{\epsilon - \epsilon_{\vec{k}}}\mathrm{Y}_\epsilon, \end{aligned} \tag{A9}$$

where $\Delta_L \equiv 2\pi/L$. Then the Kondo temperature T_K is written as $T_K = \pi V_K^2/\Delta_L$.

When the system deviates from the Toulouse point as $J_z = \frac{2\pi}{\sqrt{2}L}\gamma \to J_z = \frac{2\pi}{\sqrt{2}L}\gamma + \delta J_z$ [see Eq. (A5)], the Hamiltonian $H_{\rm EK}$ in Eq. (27) has an additional term $H_{\delta J_z}$,

$$\begin{aligned} H_{\rm EK} &\to H_{\rm EK} + H_{\delta J_z},\\ H_{\delta J_z} &= \sqrt{2}\delta J_z(\tilde{c}_d^\dagger\tilde{c}_d - 1/2)\sum_{\vec{k},\vec{k}'}\tilde{c}_{\vec{k}}^\dagger\tilde{c}_{\vec{k}'}. \end{aligned} \tag{A10}$$

We compute $dI_{\rm CD}/dV_{\rm CD}$ by treating the additional term $H_{\delta J_z}$ as a perturbation,

$$\frac{dI_{\rm CD}}{dV_{\rm CD}} \propto \frac{e^2}{h}\frac{\rho J_{P+}^2}{T_K}\left(\frac{T}{T_K}\right)^2 (\rho T)^2\left[1 - C(\pi\rho\delta J_z)^2\left(\frac{T}{T_K}\right)^2\right], \tag{A11}$$

where $C \approx 20$. The second term shows the Fermi liquid behavior originating from the deviation by δJ_z and is of higher order (sixth order) in temperature than the result at the Toulouse point (see the first term). This shows that the result of $dI_{\rm CD}/dV_{\rm CD}$ in Eq. (34) is valid also near the Toulouse point.

We compute the scaling dimension of H_{P+} and H_{Pz}. The scaling dimension ν_{P+} of H_{P+} is obtained from the relation of

$$\langle H_{P+}(t)H_{P+}(0)\rangle_{0K} \propto \frac{1}{t^{2\nu_{P+}}} \qquad (\text{at large } t). \tag{A12}$$

Here, the average $\langle\cdots\rangle_{0K}$ is obtained with respect to the Hamiltonian H_{0K}. We find $\nu_{P+} = 3$. As we consider one-dimensional reservoirs, $\nu_{P+} > 1$ implies that H_{P+} is irrelevant. Similarly, we find that the scaling dimension ν_{Pz} of H_{Pz} is 2, implying that H_{Pz} is also irrelevant. Note that the potential scattering part of H_{Pz} ($\propto \sum_{\vec{k},\vec{k}'}\tilde{c}_{{\rm C}\vec{k}}^\dagger\tilde{c}_{{\rm C}\vec{k}'} - \tilde{c}_{{\rm D}\vec{k}}^\dagger\tilde{c}_{{\rm D}\vec{k}'}$) is ignored in the computation of ν_{Pz}, because this part decouples from the quadruple dot.

[1] J. Kondo, Prog. Theor. Phys. **32**, 37 (1964).
[2] A. C. Hewson, *The Kondo problem to heavy fermions, Cambridge Studies in Magnetism* (Cambridge University Press, Cambridge, 1993).
[3] L. I. Glazman and M. E. Raikh, JETP Lett. **47**, 452 (1988).
[4] T. K. Ng and P. A. Lee, Phys. Rev. Lett. **61**, 1768 (1988).
[5] M. Pustilnik and L. Glazman, J. Phys.: Condens. Matter **16**, R513 (2004).
[6] D. Goldhaber-Gordon, H. Shtrikman, D. Mahalu, D. Abusch-Magder, U. Meirav, and M. A. Kastner, Nature (London) **391**, 156 (1998).
[7] S. M. Cronenwett, T. H. Oosterkamp, and L. P. Kouwenhoven, Science **281**, 540 (1998).
[8] W. G. van der Wiel, S. De Franceschi, T. Fujisawa, J. M. Elzerman, S. Tarucha, and L. P. Kouwenhoven, Science **289**, 2105 (2000).
[9] J. Nygard, D. H. Cobden, and P. E. Lindelof, Nature (London) **408**, 342 (2000).
[10] U. Gerland, J. von Delft, T. A. Costi, and Y. Oreg, Phys. Rev. Lett. **84**, 3710 (2000).
[11] Y. Ji, M. Heiblum, D. Sprinzak, D. Mahalu, and H. Shtrikman, Science **290**, 779 (2000).
[12] S. Takada, C. Bauerle, M. Yamamoto, K. Watanabe, S. Hermelin, T. Meunier, A. Alex, A. Weichselbaum, J. von Delft, A. Ludwig, A. D. Wieck, and S. Tarucha, Phys. Rev. Lett. **113**, 126601 (2014).
[13] E. Sela, Y. Oreg, F. von Oppen, and J. Koch, Phys. Rev. Lett. **97**, 086601 (2006).
[14] Y. Yamauchi, K. Sekiguchi, K. Chida, T. Arakawa, S. Nakamura, K. Kobayashi, T. Ono, T. Fujii, and R. Sakano, Phys. Rev. Lett. **106**, 176601 (2011).
[15] R. Potok, I. Rau, H. Shtrikman, Y. Oreg, and D. Goldhaber-Gordon, Nature (London) **446**, 167 (2007).
[16] H. T. Mebrahtu, I. V. Borzenets, H. Zheng, Y. V. Bomze, A. I. Smirnov, S. Florens, H. U. Baranger, and G. Finkelstein, Nat. Phys. **9**, 732 (2013).
[17] Z. Iftikhar, S. Jezouin, A. Anthore, U. Gennser, F. D. Parmentier, A. Cavanna, and F. Pierre, Nature (London) **526**, 233 (2015).
[18] A. J. Keller, L. Peeters, C. P. Moca, I. Weymann, D. Mahalu, V. Umansky, G. Zaránd, and D. Goldhaber-Gordon, Nature (London) **526**, 237 (2015).
[19] Z. Iftikhar, A. Anthore, A. K. Mitchell, F. D. Parmentier, U. Gennser, A. Ouerghi, A. Cavanna, C. Mora, P. Simon, and F. Pierre, Science **360**, 1315 (2018).
[20] I. Affleck and P. Simon, Phys. Rev. Lett. **86**, 2854 (2001).
[21] P. S. Cornaglia and C. A. Balseiro, Phys. Rev. Lett. **90**, 216801 (2003).
[22] J. Park, S.-S. B. Lee, Y. Oreg, and H.-S. Sim, Phys. Rev. Lett. **110**, 246603 (2013).
[23] G. Yoo, S.-S. B. Lee, and H.-S. Sim, Phys. Rev. Lett. **120**, 146801 (2018).
[24] I. Affleck, *Perspectives of Mesoscopic Physics* (World Scientific, Singapore, 2010), pp. 1–44.
[25] S.-S. B. Lee, J. Park, and H.-S. Sim, Phys. Rev. Lett. **114**, 057203 (2015).

[26] J. Shim, H.-S. Sim, and S.-S. B. Lee, Phys. Rev. B **97**, 155123 (2018).
[27] I. V. Borzenets, J. Shim, J. Chen, A. Ludwig, A. Wieck, S. Tarucha, H.-S. Sim, and M. Yamamoto, Nature (London) **579**, 210 (2020).
[28] R. Sakano and N. Kawakami, Phys. Rev. B **72**, 085303 (2005).
[29] R. Zitko, J. Bonca, A. Ramsak, and T. Rejec, Phys. Rev. B **73**, 153307 (2006).
[30] T. Kuzmenko, K. Kikoin, and Y. Avishai, Phys. Rev. B **73**, 235310 (2006).
[31] A. K. Mitchell, T. F. Jarrold, and D. E. Logan, Phys. Rev. B **79**, 085124 (2009).
[32] D. E. Liu, S. Chandrasekharan, and H. U. Baranger, Phys. Rev. Lett. **105**, 256801 (2010).
[33] P. P. Baruselli, R. Requist, M. Fabrizio, and E. Tosatti, Phys. Rev. Lett. **111**, 047201 (2013).
[34] M. Seo, H. K. Choi, S.-Y. Lee, N. Kim, Y. Chung, H.-S. Sim, V. Umansky, and D. Mahalu, Phys. Rev. Lett. **110**, 046803 (2013).
[35] S. Amasha, A. J. Keller, I. G. Rau, A. Carmi, J. A. Katine, H. Shtrikman, Y. Oreg, and D. Goldhaber-Gordon, Phys. Rev. Lett. **110**, 046604 (2013).
[36] G. Yoo, J. Park, S.-S. B. Lee, and H.-S. Sim, Phys. Rev. Lett. **113**, 236601 (2014).
[37] Y. Chung, J. Choi, and H.-S. Sim, J. Korean Phy. Soc. **72**, 1454 (2018).
[38] P. W. Anderson, Phys. Rev. Lett. **34**, 953 (1975).
[39] M. E. Raikh, L. I. Glazman, and L. E. Zhukov, Phys. Rev. Lett. **77**, 1354 (1996).
[40] A. Taraphder and P. Coleman, Phys. Rev. Lett. **66**, 2814 (1991).
[41] M. C. Rogge and R. J. Haug, Phys. Rev. B **77**, 193306 (2008).
[42] C. Hong, G. Yoo, J. Park, M.-K. Cho, Y. Chung, H.-S. Sim, D. Kim, H. Choi, V. Umansky, and D. Mahalu, Phys. Rev. B **97**, 241115(R) (2018).
[43] P. S. Cornaglia, H. Ness, and D. R. Grempel, Phys. Rev. Lett. **93**, 147201 (2004).
[44] J. Koch, M. E. Raikh, and F. von Oppen, Phys. Rev. Lett. **96**, 056803 (2006).
[45] J. Koch, E. Sela, Y. Oreg, and F. von Oppen, Phys. Rev. B **75**, 195402 (2007).
[46] V. Oganesyan, S. Kivelson, T. Geballe, and B. Moyzhes, Phys. Rev. B **65**, 172504 (2002).
[47] V. I. Kozub, A. V. Lopatin, and V. M. Vinokur, Phys. Rev. Lett. **90**, 226805 (2003).
[48] M. Dzero and J. Schmalian, Phys. Rev. Lett. **94**, 157003 (2005).
[49] Y. Matsushita, H. Bluhm, T. H. Geballe, and I. R. Fisher, Phys. Rev. Lett. **94**, 157002 (2005).
[50] S. Andergassen, T. A. Costi, and V. Zlatic, Phys. Rev. B **84**, 241107(R) (2011).
[51] T. A. Costi and V. Zlatic, Phys. Rev. Lett. **108**, 036402 (2012).
[52] G. E. Prawiroatmodjo, M. Leijnse, F. Trier, Y. Chen, D. V. Christensen, M. Soosten, N. Pryds, and T. S. Jespersen, Nat. Commun. **8**, 395 (2017).
[53] T.-F. Fang, A.-M. Guo, H.-T. Lu, H.-G. Luo, and Q.-F. Sun, Phys. Rev. B **96**, 085131 (2017).
[54] A. Hamo, A. Benyamini, I. Shapir, I. Khivrich, J. Waissman, K. Kaasbjerg, Y. Oreg, F. von Oppen, and S. Ilani, Nature (London) **535**, 395 (2016).
[55] J. Schrieffer and P. Wolff, Phys. Rev. **149**, 491 (1966).
[56] P. Anderson, J. Phys. C **3**, 2436 (1970).
[57] A. P. Jauho, N. S. Wingreen, and Y. Meir, Phys. Rev. B **50**, 5528 (1994).
[58] P. Nozieres, J. Low Temp. Phys. **17**, 31 (1974).
[59] A. Kaminski, Y. V. Nazarov, and L. I. Glazman, Phys. Rev. B **62**, 8154 (2000).
[60] G. Zarand and J. von Delft, Phys. Rev. B **61**, 6918 (2000).
[61] M. R. Graber, W. A. Coish, C. Hoffmann, M. Weiss, J. Furer, S. Oberholzer, D. Loss, and C. Schonenberger, Phys. Rev. B **74**, 075427 (2006).
[62] S. J. Chorley, M. R. Galpin, F. W. Jayatilaka, C. G. Smith, D. E. Logan, and M. R. Buitelaar, Phys. Rev. Lett. **109**, 156804 (2012).
[63] C. Mora, Phys. Rev. B **80**, 125304 (2009).
[64] I. Affleck and A. W. W. Ludwig, Phys. Rev. B **48**, 7297 (1993).
[65] B. A. Jones and C. M. Varma, Phys. Rev. B **40**, 324 (1989).
[66] I. Affleck, A. W. W. Ludwig, H.-B. Pang, and D. L. Cox, Phys. Rev. B **45**, 7918 (1992).
[67] M. Fabrizio, A. O. Gogolin, and P. Nozieres, Phys. Rev. Lett. **74**, 4503 (1995).
[68] M. Pustilnik, L. Borda, L. I. Glazman, and J. von Delft, Phys. Rev. B **69**, 115316 (2004).
[69] S. M. Tabatabaei, Phys. Rev. B **97**, 235131 (2018).